<div style="border:1px solid">
Banner appropriate to article type will appear here in typeset article
</div>

Asynchronous and synchronous quenching of a globally unstable jet via axisymmetry breaking

Abhijit K. Kushwaha[1]†**, Nicholas A. Worth**[2]**, James R. Dawson**[2]**, Vikrant Gupta**[3] **and Larry K. B. Li**[1]‡

[1]Department of Mechanical and Aerospace Engineering, The Hong Kong University of Science and Technology, Clear Water Bay, Hong Kong

[2]Department of Energy and Process Engineering, Norwegian University of Science and Technology, Trondheim, Norway

[3]Department of Mechanics and Aerospace Engineering, Southern University of Science and Technology, Shenzhen, China

We explore whether axisymmetry breaking can be exploited for the open-loop control of a prototypical hydrodynamic oscillator, namely a low-density inertial jet exhibiting global self-excited axisymmetric ($m = 0$) oscillations. Adopting a forced synchronization framework, we experimentally subject the jet to transverse (antisymmetric) and axial (symmetric) forcing by placing it, respectively, at the pressure node and antinode of a planar acoustic standing wave. We find that when forced transversely or axially at a low amplitude, the jet always transitions first from a period-1 limit cycle to $\mathbb{T}^2$ quasiperiodicity via a Neimark–Sacker bifurcation. However, we find that the subsequent transition, from $\mathbb{T}^2$ quasiperiodicity to 1:1 lock-in, depends on the spatial symmetry of the applied perturbations: axial forcing induces a saddle-node bifurcation at small detuning but an inverse Neimark–Sacker bifurcation at large detuning, whereas transverse forcing always induces an inverse Neimark–Sacker bifurcation irrespective of the detuning. Nevertheless, we find that the shape and position of the Arnold tongue remain similar for both types of forcing. This shows that although transverse and axial forcing are equally capable of causing lock-in, only transverse forcing can ensure that it occurs via the suppression route rather than the phase-locking route. In this way, transverse forcing enables both asynchronous and synchronous quenching of the natural mode to occur without resonant or non-resonant amplification of the forced mode, resulting in substantially lower values of the overall response amplitude across all detuning values. From this, we conclude that breaking the jet axisymmetry via transverse forcing is a more effective open-loop control strategy than preserving the jet axisymmetry via axial forcing. Finally, we show that the observed synchronization phenomena can be qualitatively modelled with just two coupled Van der Pol oscillators forced externally by sinusoidal terms. The success of such a simple low-dimensional model in capturing the complex synchronization dynamics of a multi-modal hydrodynamic system opens up new opportunities for axisymmetry breaking to be exploited for the open-loop control of other globally unstable flows.

† Email address for correspondence: akkushwaha@connect.ust.hk
‡ Email address for correspondence: larryli@ust.hk

Abstract must not spill onto p.2

2   *A. K. Kushwaha, N. A. Worth, J. R. Dawson, V. Gupta and L. K. B. Li*

1. Introduction

Open jet flows are ubiquitous in nature and engineering. Over the years, their spatiotemporal stability and dynamics have been extensively studied (Huerre & Monkewitz 1990; Schmid & Henningson 2001; Drazin & Reid 2004). It is now well known that when the density of a jet is sufficiently below that of its surroundings, a region of local absolute instability can develop in the near field (Monkewitz & Sohn 1988; Yu & Monkewitz 1990; Jendoubi & Strykowski 1994; Lesshafft & Huerre 2007; Coenen *et al.* 2008; Lesshafft & Marquet 2010; Srinivasan *et al.* 2010; Coenen & Sevilla 2012). If this region is sufficiently large, it can give rise to global instability, causing the jet to transition from a spatial amplifier of extrinsic perturbations to a self-excited oscillator with an intrinsic limit cycle at a well-defined natural frequency (Chomaz *et al.* 1988; Chomaz 2005; Lesshafft *et al.* 2006; Hallberg *et al.* 2007; Lesshafft *et al.* 2007; Coenen *et al.* 2017; Chakravarthy *et al.* 2018). If the jet discharges from a round non-swirling nozzle with sufficiently thin shear layers, its dynamics will be dominated by axisymmetric (bulging) oscillations with an azimuthal wavenumber of $m = 0$, which can arise via a supercritical or subcritical Hopf bifurcation (Sreenivasan *et al.* 1989; Monkewitz *et al.* 1990; Kyle & Sreenivasan 1993; Hallberg & Strykowski 2006; Zhu *et al.* 2017, 2019). Such self-excited oscillations are desirable in some situations because they can aid mixing and transport. They are, however, undesirable in other situations because they can couple with structural, acoustic or other hydrodynamic modes at nearby frequencies. It is thus important to be able to control the self-excited oscillations of globally unstable jets.

   Studies have already shown that globally unstable axisymmetric jets can be readily controlled with time-periodic acoustic forcing applied axially, such that rotationally symmetric perturbations of a prescribed frequency and amplitude are generated at the jet base (see §1.2 for details). Under most conditions, however, such jets are not only globally unstable to the axisymmetric mode ($m = 0$), but are also convectively unstable to the helical modes, i.e. the spiralling modes with $m = \pm1, \pm2, \ldots$ (Monkewitz & Sohn 1988; Jendoubi & Strykowski 1994; Lesshafft & Huerre 2007; Coenen *et al.* 2008). Consequently, it is important to explore the effects of rotationally asymmetric forcing as well, not least because such forcing could interact differently with the natural axisymmetric and helical modes, producing axisymmetry-breaking phenomena not seen with purely axial forcing. In this study, we take a forced synchronization approach to investigating the effects of axisymmetry breaking, induced by transverse acoustic forcing, on a globally unstable low-density jet oscillating self-excitedly in a period-1 limit cycle. Before presenting our experimental and modelling methodologies (§2 and §3) and results (§4 and §5), we will review the universal concept of forced synchronization and its amplitude suppression mechanisms (§1.1) and survey previous work on the axial (§1.2) and transverse (§1.3) forcing of axisymmetric jets, drawing on examples involving global instability in the hydrodynamic field whenever possible.

1.1. *Forced synchronization and its amplitude suppression mechanisms*

When a self-excited oscillator (e.g. a globally unstable flow) is externally forced at a frequency f_f different from its natural frequency f_n, it can adjust its motion to match that of the forcing signal (Pikovsky *et al.* 2003). This unidirectional adjustment process is known as *forced synchronization* (Balanov *et al.* 2009) and can lead to a completely synchronous state, known as *lock-in* in fluid mechanics (Sreenivasan *et al.* 1989), if the forcing amplitude is sufficiently high. According to synchronization theory based on single-mode oscillators, lock-in tends to occur via two universal routes (Balanov *et al.* 2009): phase locking and suppression.

Quenching of a globally unstable jet via axisymmetry breaking   3

Along the phase-locking route, which typically arises when the detuning ($|f_f - f_n|$) is small, lock-in occurs via a gradual pulling of f_n^* (where the superscript * denotes the presence of external forcing) towards f_f as the forcing amplitude increases. By contrast, along the suppression route, which typically arises when the detuning is large, lock-in occurs via a gradual reduction in the amplitude of the natural mode without a simultaneous pulling of its frequency. These two routes can also be distinguished by their unique bifurcations: the phase-locking route involves a saddle-node bifurcation to lock-in, whereas the suppression route involves an inverse Neimark–Sacker bifurcation to lock-in, i.e. a torus-death bifurcation (Balanov *et al.* 2009; Li & Juniper 2013*a*,*c*; Hyodo & Biwa 2018; Kashinath *et al.* 2018).

However, only along the suppression route can *asynchronous quenching* occur (Bogoliubov & Mitropolsky 1961; Balanov *et al.* 2009). This is a nonlinear phenomenon whereby the natural mode of a self-excited oscillator is stabilised to a fixed point by periodic forcing applied externally at an off-resonance frequency sufficiently far from f_n, i.e. at large detuning (Minorsky 1974). Under most conditions, asynchronous quenching occurs without amplification of the forcing signal (Minorsky 1967), resulting in a substantial reduction in the overall response amplitude of the forced self-excited system – often to less than 20% of the natural (uncontrolled) amplitude (Guan *et al.* 2019*a*,*b*). Such quenching of the natural mode is due to the external forcing inducing an asymptotic loss of stability in the original limit-cycle attractor (Minorsky 1974). Nevertheless, it is worth noting that quenching of the natural mode can occur for small detuning as well, in an analogous process known as *synchronous quenching* (Odajima *et al.* 1974). This type of quenching, however, is usually accompanied by resonant amplification of the forcing signal, resulting in an increase in the overall response amplitude (Abel *et al.* 2009). Both asynchronous and synchronous quenching are universal phenomena in nonlinear dynamical systems (Pikovsky *et al.* 2003) and can be modelled with a forced self-excited oscillator containing a generic Van der Pol (VDP) kernel (Dewan 1972; Odajima *et al.* 1974). Unsurprisingly, such quenching phenomena have been observed in various self-excited systems, ranging from premixed combustors (Lubarsky *et al.* 2003; Bellows *et al.* 2008; Kashinath *et al.* 2018; Guan *et al.* 2018, 2019*a*,*c*,*b*; Mondal *et al.* 2019; Roy *et al.* 2020) to plasma columns (Keen & Fletcher 1969, 1970; Ohe & Takeda 1974) to open jet flows (Staubli & Rockwell 1987; Li & Juniper 2013*a*), albeit mostly in response to purely axial (symmetric) forcing.

For open-loop control, asynchronous quenching appears to be a promising mechanism by which to suppress limit-cycle oscillations. However, a major drawback of this strategy, as implemented in the examples above, is the need for f_f to be sufficiently far from f_n (Bogoliubov & Mitropolsky 1961; Minorsky 1967). This presents a potential challenge for open-loop controllers as it requires prior knowledge of the value of f_n, which may be difficult to obtain in systems where even momentary excursions into a high-amplitude limit-cycle regime can cause catastrophic mechanical or thermal damage. Exacerbating this is the possibility that f_n can drift with changes in the operating conditions or system parameters. For robust control, it would be helpful to have a method of suppressing limit-cycle oscillations that is less sensitive to the detuning between the forced and natural modes. In other words, we seek a method of inducing both asynchronous and synchronous quenching that simultaneously avoids any amplification of the forcing signal. In this study, we demonstrate on a prototypical hydrodynamic oscillator – a globally unstable low-density axisymmetric jet – that one such method is to exploit axisymmetry breaking by applying transverse acoustic forcing.

1.2. *Axial forcing of globally unstable jets*

The hydrodynamic response of a globally unstable low-density axisymmetric jet to axial acoustic forcing has been studied by Li & Juniper (2013*a*,*c*). These researchers found that, when f_f is incommensurable with f_n^* (i.e. when the dressed winding number, f_n^*/f_f, is

4   *A. K. Kushwaha, N. A. Worth, J. R. Dawson, V. Gupta and L. K. B. Li*

irrational), the jet can be in one of three possible states depending on the forcing amplitude: (i) when unforced, the jet oscillates periodically at f_n, with its phase trajectory evolving on a limit-cycle attractor; (ii) when forced weakly, the jet oscillates quasiperiodically at both f_n^* and f_f, with its phase trajectory evolving on a two-frequency torus attractor; and (iii) when forced strongly, the jet locks into the forcing by oscillating only at f_f and its harmonics, with the phase trajectory evolving on another limit-cycle attractor but at f_f instead of f_n. The minimum forcing amplitude required for lock-in increases as f_f shifts away from f_n, producing a ∨-shaped lock-in boundary centred on $f_f/f_n = 1$. The parameter space above this boundary is known as the 1:1 Arnold tongue in synchronization theory (Pikovsky *et al.* 2003; Balanov *et al.* 2009). Such a tongue can be found not only in low-density jets (Sreenivasan *et al.* 1989; Kyle & Sreenivasan 1993; Hallberg & Strykowski 2008; Li & Juniper 2013a,c; Murugesan *et al.* 2019) but also in other globally unstable flows, such as bluff-body wakes (Koopmann 1967; Stansby 1976; Provansal *et al.* 1987; Olinger & Sreenivasan 1988; Karniadakis & Triantafyllou 1989), capillary jets (Olinger 1992), jet diffusion flames (Juniper *et al.* 2009; Li & Juniper 2013b), and cross-flow jets (Davitian *et al.* 2010a,b; Karagozian 2010; Shoji *et al.* 2020).

   Li & Juniper (2013a,c) also found that, as the forcing amplitude increases en route to lock-in, the jet follows either the phase-locking route if f_f is close to f_n, or the suppression route if f_f is far from f_n. Crucially, asynchronous quenching was observed only along the suppression route (Li & Juniper 2013a,c). All of these experimental observations are consistent with theoretical analyses of the classic (single-mode) VDP oscillator subjected to external periodic forcing (Dewan 1972; Balanov *et al.* 2009). This shows that these synchronization phenomena are not unique to a forced low-density jet, but are universal to forced self-excited oscillators in general.

1.3. *Transverse forcing of jets*

Compared with that of axial forcing, the effect of transverse forcing has been less well studied, despite its relevance to annular combustors in gas turbines (Hauser *et al.* 2010; Bauerheim *et al.* 2014; Bourgouin *et al.* 2015; Ghirardo *et al.* 2016). In such devices, multiple jet-stabilised flames are typically distributed around the annulus and can interact with the acoustics therein to produce azimuthal thermoacoustic instabilities in the form of spinning and standing modes (Ghirardo & Juniper 2013; Noiray & Schuermans 2013b; Bothien *et al.* 2015; Yang *et al.* 2019). From the local viewpoint of an individual flame, such modes appear as an approximately one-dimensional acoustic field, generating time-varying pressure gradients in a direction perpendicular (transverse) to the jet axis (O'Connor *et al.* 2015). Under certain conditions, a statistical preference can emerge for standing modes over spinning modes (Noiray *et al.* 2011; Wolf *et al.* 2012; Worth & Dawson 2013). Flames located at different points along the standing waveform would thus experience different pressure fields, causing some hydrodynamic modes to be preferentially excited over others, depending on the exact nozzle location (Lespinasse *et al.* 2013).

   Lieuwen's group (O'Connor & Lieuwen 2011, 2012; Blimbaum *et al.* 2012; O'Connor *et al.* 2015; Smith *et al.* 2018b,a) has investigated the response of swirling jets and swirl-stabilised flames to planar acoustic standing waves. At a pressure node, the acoustic perturbations are antisymmetric (out-of-phase by π) about the nodal line running through the nozzle centre, producing transverse velocity perturbations that preferentially excite the odd-m helical hydrodynamic modes ($m = \pm 1, \pm 3, \ldots$; O'Connor & Lieuwen 2012; O'Connor & Lieuwen 2012; Smith *et al.* 2018b); the superposition of a pair of counter-rotating $m = \pm 1$ modes of equal amplitude can induce a transverse flapping motion with staggered vortices in the shear layers. At a pressure antinode, the acoustic perturbations are symmetric (in-phase) about the antinodal line running through the nozzle centre, producing axial velocity perturbations that

preferentially excite the bulging hydrodynamic mode ($m = 0$), leading to the axisymmetric roll-up of vortical structures (O'Connor & Lieuwen 2012; O'Connor & Lieuwen 2012; Smith *et al.* 2018*b*). From these and other related studies (Hauser *et al.* 2010; Lespinasse *et al.* 2013; Saurabh & Paschereit 2017; Saurabh *et al.* 2017), it can be concluded that axial forcing (pressure antinode) preferentially excites axisymmetric flow structures, whereas transverse forcing (pressure node) preferentially excites flapping flow structures.

The hydrodynamic response of a globally unstable jet to transverse acoustic forcing has been studied by only a few researchers. In seminal experiments, O'Connor & Lieuwen (2012) applied transverse (out-of-phase) and axial (in-phase) forcing to a swirling annular jet featuring a central vortex breakdown bubble generated by global hydrodynamic instability. When unforced, the jet was found to be dominated by the $m = -2$ and -1 helical modes, which were associated with large-scale undulations of the jet column and with coherent structures in the recirculation zone, respectively. Transverse forcing was found to alter the relative amplitudes of the two modes, without much affecting the axisymmetric mode ($m = 0$). These findings are consistent with the trends discussed above, highlighting again how certain hydrodynamic modes can be preferentially excited over others, depending on the spatial symmetry of the applied forcing. Crucially, in this non-axisymmetric swirling jet, neither lock-in nor asynchronous/synchronous quenching was observed with either axial or transverse forcing, even at high forcing amplitudes (O'Connor & Lieuwen 2012).

Other studies that have examined the effects of asymmetric forcing have done so with a focus on convectively unstable jets (Parekh *et al.* 1987; Reynolds *et al.* 2003; Suzuki *et al.* 2004; Tyliszczak & Geurts 2014; Tyliszczak 2015; Gohil & Saha 2019). Unlike globally unstable jets, convectively unstable jets are not self-excited (Huerre & Monkewitz 1990) and therefore cannot undergo asynchronous or synchronous quenching, regardless of the value of f_f (Minorsky 1967). Studies on convectively unstable axisymmetric jets have examined how some of their characteristics – such as mixing, entrainment, and spreading – can be enhanced via transverse forcing (Urbin & Métais 1997; Danaila & Boersma 2000; Worth *et al.* 2020; Douglas *et al.* 2021) or via a combination of axial and transverse forcing applied at the same frequency (Æsøy *et al.* 2021) or at different frequencies (Da Silva & Métais 2002). However, little is known about how such complex forcing patterns would affect a globally unstable axisymmetric jet, particularly its bifurcations en route to lock-in and its ability to undergo asynchronous and synchronous quenching. This is despite the fact that such a jet is a prototypical hydrodynamic oscillator (Huerre & Monkewitz 1990) and that global instability has been detected in the open shear flows of various propulsion and power-generation devices (Juniper 2012; Oberleithner *et al.* 2015; Tammisola & Juniper 2016).

1.4. *Contributions of the present study*

It is well known that a low-density inertial jet discharging from a round nozzle can develop global axisymmetric oscillations at a discrete natural frequency f_n (§1). Previous experiments have shown that when such a jet is forced axially at an off-resonance frequency f_f, its self-excited oscillations can become suppressed via asynchronous quenching, without amplification of the forcing signal, resulting in a substantial reduction in the overall response amplitude (§1.1 and §1.2). This is clearly a promising strategy for open-loop flow control, but it requires f_f to be sufficiently far from f_n. In this study, we propose an alternative method of inducing both asynchronous and synchronous quenching, one that exploits axisymmetry breaking to avoid any amplification of the forcing signal, thus removing the need to worry about the exact detuning between f_f and f_n. Specifically, we ask three research questions:

(i) *Can breaking the axisymmetry of a globally unstable jet via transverse forcing lead to a more effective open-loop control strategy than preserving the axisymmetry via axial forcing?*

6   *A. K. Kushwaha, N. A. Worth, J. R. Dawson, V. Gupta and L. K. B. Li*
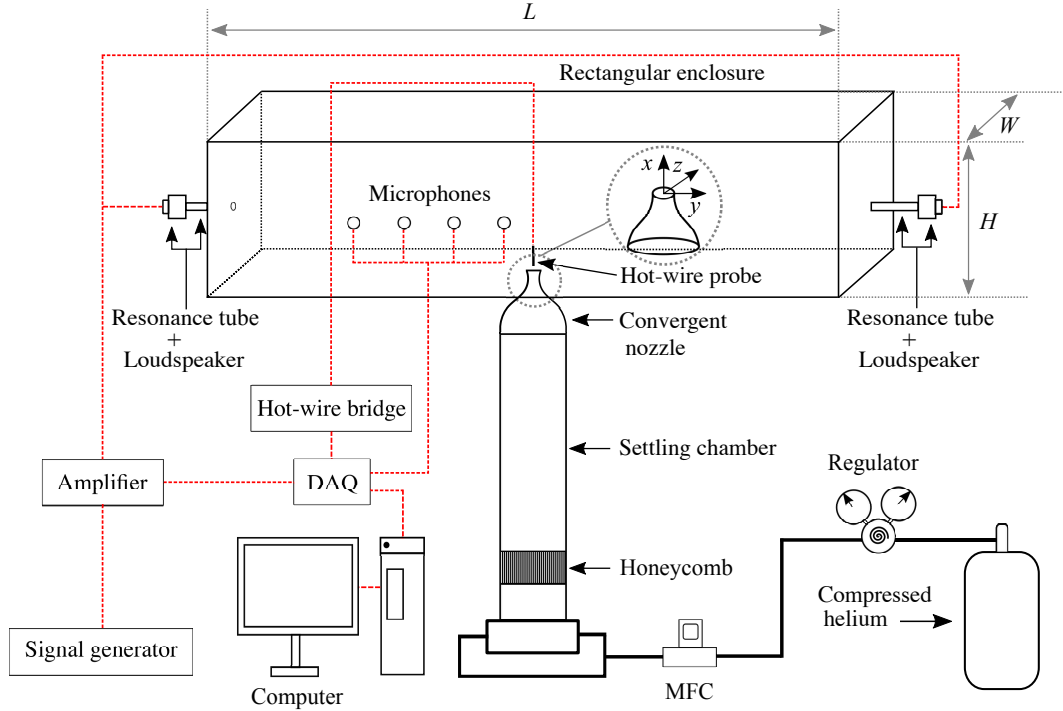

Figure 1: Diagram of the experimental set-up. The measurement diagnostics include four microphones mounted flush along the transverse wall of the enclosure, a hot-wire probe positioned on the jet centreline, and a PIV system (not shown). MFC: mass flow controller. DAQ: data acquisition system.

(ii) *If it can, how do the synchronization phenomena – such as the bifurcation routes, Arnold tongues, and quenching mechanisms – differ between transverse and axial forcing?*

(iii) *Can these synchronization phenomena be modelled phenomenologically with a low-dimensional system based simply on a pair of coupled VDP oscillators?*

The rest of this paper is organised as follows. In §2 and §3, we introduce the experimental set-up and low-dimensional model, respectively. In §4 and §5, we experimentally investigate the effects of axisymmetry breaking on a globally unstable low-density jet, and then we model the main synchronization phenomena, such as the bifurcation routes, Arnold tongues, and quenching mechanisms. In §6, we conclude with the key implications of this study for the open-loop control of globally unstable axisymmetric flows.

2. Experimental set-up

The experimental set-up consists of two main components (figure 1): a convergent nozzle from which a globally unstable axisymmetric jet is produced (§2.1), and a rectangular enclosure in which planar acoustic standing waves are established to perturb the jet (§2.2).

2.1. *Jet nozzle and velocity measurements*

The nozzle has a round outlet whose exit diameter is $D = 6$ mm. Its internal walls are defined by a fifth-order polynomial with a 34:1 area contraction between the settling chamber and the nozzle outlet. The streamwise, transverse (radial) and cross-stream coordinates are denoted by x, y and z, respectively, as shown in figure 1. The nozzle outlet can be moved along the transverse (y) direction, enabling the jet position to be varied relative to the standing acoustic waveform in the enclosure. However, the nozzle outlet always protrudes $1.67D$ into the enclosure itself so as to minimize wall effects. Helium gas is discharged from the
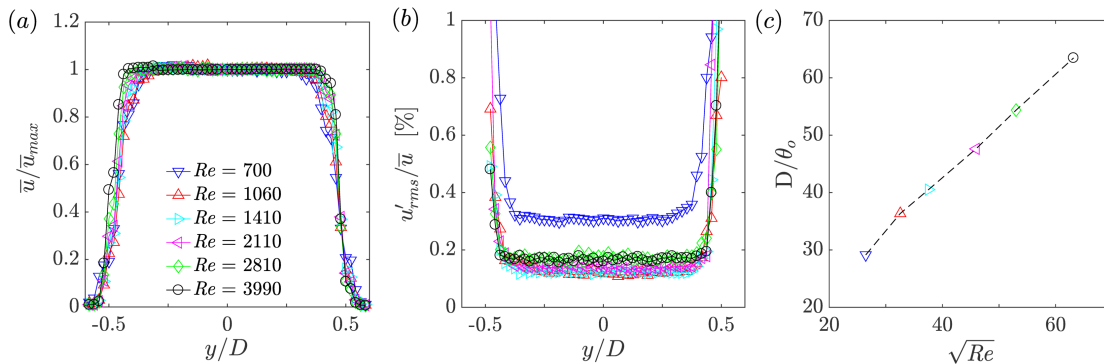
Figure 2: Characterization of the jet base flow: (a) normalized time-averaged streamwise velocity and (b) its local fluctuations, both as a function of the radial position. Also shown is (c) the transverse curvature as a function of the square root of the Reynolds number. The data are acquired with a hot-wire anemometer positioned just beyond the nozzle outlet ($x/D \approx 0.1$).

nozzle into the enclosure air (at a temperature of 293 K), creating a jet whose density ratio is $S \equiv \rho_j / \rho_\infty = 0.14$, well below the upper limit for global instability (Monkewitz *et al.* 1990; Kyle & Sreenivasan 1993). The helium is supplied from a compressed gas cylinder and is metered with a mass flow controller (Alicat MCR-500). Figure 2(a) shows radial profiles of the normalized time-averaged streamwise velocity, $\overline{u}/\overline{u}_{max}$, for a range of Reynolds numbers, $700 \leqslant Re \equiv U_j \rho_j D / \mu_j \leqslant 3990$, where U_j is the jet centreline velocity and μ_j is the jet dynamic viscosity. The data are acquired with a hot-wire anemometer positioned just beyond the nozzle outlet ($x/D \approx 0.1$); the measurement procedures are described further below. It can be seen in figure 2(a) that the velocity profile is top-hat with thin shear layers. This aids the detection of global instability by keeping the critical *Re* low, thus limiting the ability of convective modes to amplify inherent disturbances (Hallberg *et al.* 2007). Figure 2(b) shows that the velocity fluctuations in the jet core are weak ($u'_{rms}/\overline{u} < 0.35\%$), while figure 2(c) shows that the transverse curvature – defined as D normalized by the initial momentum thickness θ_0 – scales linearly with $Re^{1/2}$. This linear scaling indicates that the initial shear layers are laminar, which further aids the detection of global instability.

The hydrodynamic response of the jet to acoustic perturbations is characterized with hot-wire anemometry (HWA) and particle image velocimetry (PIV). HWA is used when long time traces are needed to identify the topology of the jet attractor in its reconstructed phase space, whereas PIV is used when spatiotemporal information is needed to better understand the flow symmetry. The HWA system consists of a constant-temperature bridge operated at an overheat ratio of 1.8 and connected to a single-normal probe (Dantec 55P11) equipped with a platinum-plated tungsten wire (diameter: 5 μm; length: 1.25 mm). Its frequency response is around 10^4 Hz, well above the natural global frequency of the jet (§4: $f_n \sim 10^3$ Hz). Previous studies have shown that when an open shear flow becomes globally unstable, a large section of its domain becomes temporally synchronized such that its dynamics can be resolved with only local measurements taken at a single spatial location (Huerre & Monkewitz 1990; Broze & Hussain 1994). In both the unforced (§4) and forced (§5) jet experiments, the HWA probe is positioned on the jet centreline, $1.5D$ downstream of the nozzle outlet, i.e. at $(x/D, y/D) = (1.5, 0)$, with an uncertainty of $\pm 0.017D$ in each axis. This sampling location is chosen because it is far enough downstream for a nonlinear global mode to emerge and interact with the applied forcing (Hallberg & Strykowski 2008), but it is not so far downstream as to be outside the potential core, where fluctuations in helium concentration could contaminate the HWA data (Li & Juniper 2013*a,c*). Furthermore, sampling the HWA data in the potential core is preferred because it

8   *A. K. Kushwaha, N. A. Worth, J. R. Dawson, V. Gupta and L. K. B. Li*

provides direct measurements of the wavemaker (Lesshafft *et al.* 2006; Qadri *et al.* 2018), which is the flow region that prescribes the intrinsic dynamics of the global mode (Huerre & Monkewitz 1990; Chomaz 2005). The HWA probe wire itself is oriented parallel to the z axis (see figure 1) so that it simultaneously senses both streamwise (x) and transverse (y) velocity components. This probe orientation enables both axisymmetric ($m = 0$) and transverse flapping ($m = \pm 1$) oscillations in the jet to be resolved. For each test run, the HWA voltage is digitized at 25600 Hz for 8 s on a 16-bit data acquisition system, generating a time trace of the local x–y velocity, $\gamma(t)$. Here the conventional symbol for velocity, $u(t)$, is not used because it is reserved for the x velocity component measured with PIV (see below) and because the HWA probe is sensitive to both the x and y velocity components. The $\gamma(t)$ data are examined via (i) the power spectral density (PSD), as computed with the algorithm of Welch (1967); (ii) the instantaneous phase difference, as computed with the Hilbert transform, and (iii) the phase space, as reconstructed via nonlinear time series analysis based on the time-delay embedding theorem of Takens (1981) (Appendix A).

Planar stereoscopic time-resolved PIV measurements are performed to quantify the spatiotemporal evolution of the jet velocity under different forcing conditions. The PIV system consists of a high-speed dual-cavity Nd:YLF laser (Litron LDY303HE), a set of sheet-forming optics (Thorlabs), and two high-speed cameras (Photron FASTCAM SA1.1). Both cameras are fitted with Scheimpflug adapters and 180 mm lenses, with their axes aligned at 12.5° to the measurement plane normal. The measurement plane itself is illuminated with a laser sheet (thickness: 1 mm) positioned in the x–y plane. Oil-droplet seeding is introduced into both the jet flow and the enclosure air via a Laskin nozzle. Image pairs are recorded at 5442 Hz, which is more than five times f_n; the image separation time is $\delta t = 12\ \mu$s. The image resolution is 768 (height) × 512 (width) pixels at a depth of 12 bits, spread over a field-of-view of $4.44D \times 2.96D$. The image pairs are processed with the software DaVis 8.2.2 from LaVision. First, the image pairs are preprocessed with two filters: (i) a sliding background subtraction filter with a width of 32 pixels, and (ii) a particle intensity normalization filter with a width of 8 pixels. Next, the image pairs are processed with a multipass cross-correlation algorithm. The initial interrogation area contains 64×64 pixels, with a 50% window overlap for the first two passes. The final interrogation area contains 32×32 pixels, which corresponds to 1.11×1.11 mm in physical space; the window overlap for the last pass is 75%, producing a final vector spacing of $0.046D$. The velocity components in the streamwise (x), transverse (y) and cross-stream (z) directions are denoted by u, v and w, respectively, with the magnitude of the total velocity vector given by $V \equiv \sqrt{u^2 + v^2 + w^2}$. In each test run, 4000 image pairs are recorded, resulting in the same number of instantaneous vector fields. This represents over 650 cycles of the natural jet oscillation at f_n, which is sufficient for statistical convergence.

2.2. *Acoustic pressure field*

As mentioned earlier, the jet discharges into a rectangular enclosure, in which planar acoustic standing waves are established to perturb the jet. These waves arise from resonance between the natural acoustic modes of the enclosure and the pressure oscillations generated by a pair of loudspeakers (Monacor KU-516) mounted at opposite ends of the enclosure (figure 1). Each loudspeaker is fitted with its own acoustic resonance tube and is driven by a sinusoidal voltage signal sent from a function generator (Aim–TTi TGA1244) via a power amplifier (Crown CE1000). The frequency of the signal (i.e. the forcing frequency f_f) is varied around the natural global frequency of the jet ($0.8 \leqslant f_f/f_n \leqslant 1.2$) in order to explore the 1:1 Arnold tongue and its synchronization phenomena. The enclosure has a width of $W = 0.22$ m (z direction), a height of $H = 0.59$ m (x direction), and a variable length of $L = 0.96$–1.35 m
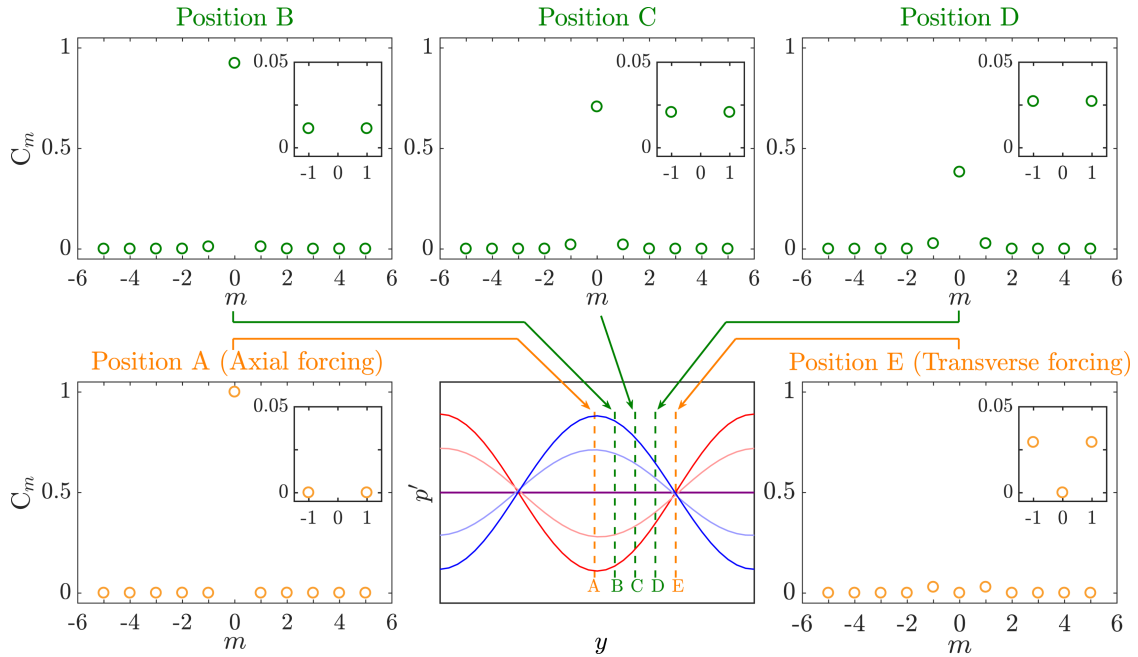
Figure 3: Decomposition of the acoustic pressure field in the jet enclosure. The modal amplitude is shown as a function of m at five different locations in a planar acoustic standing wave: a pressure antinode (position $\mathbb{A}$), a pressure node (position $\mathbb{E}$), and between a pressure antinode and node (positions $\mathbb{B}$, $\mathbb{C}$, and $\mathbb{D}$). At the pressure node (position $\mathbb{E}$), the superposition of the $m = \pm 1$ helical modes leads to a transverse flapping motion. In the experiments, three full standing waves are present in the jet enclosure but, for illustration purposes, only one is shown here.

(y direction) so that the acoustic resonance frequency can be carefully tuned to match f_f. The ratio of the enclosure width to the jet diameter ($W/D = 36.7$) is large enough to keep confinement effects negligible in the near field, $0 \leqslant x/D \leqslant 4$. At every value of f_f, the enclosure contains three full standing waves. The wavelength of these transverse acoustic waves is much larger than the jet diameter ($\lambda/D > 53.5$), implying that the jet can be regarded as acoustically compact in the near field. The acoustic pressure fluctuations (p') in the enclosure are measured with four microphones (B&K Type 4939-A-011: $\pm 2.07 \times 10^{-5}$ Pa uncertainty, 4.13 mV Pa^{-1} sensitivity) mounted flush along the transverse wall (figure 1). The multiple microphone method is used to reconstruct the acoustic field in the enclosure from estimates of the incident (p_i) and reflected (p_r) planar acoustic waves (Seybert & Ross 1977; Jang & Ih. 1998). The stationarity of the acoustic mode is verified by ensuring that the standing-wave ratio is sufficiently close to zero: $-0.01 < (|p_i| - |p_r|)/(|p_i| + |p_r|) < 0.01$. The jet is positioned at five discrete locations along the acoustic standing wave, producing a variety of forcing conditions: pure axial forcing (position $\mathbb{A}$ in figure 3: a pressure antinode), pure transverse forcing (position $\mathbb{E}$: a pressure node), and combinations of axial and transverse forcing (positions $\mathbb{B}$, $\mathbb{C}$ and $\mathbb{D}$: between a pressure antinode and a pressure node).

As discussed in §1.3, placing a jet in an acoustic standing wave can preferentially excite certain hydrodynamic modes, depending on the exact nozzle location. Following O'Connor *et al.* (2015), we use the Jacobi–Anger expansion to decompose the planar acoustic perturbations in the jet enclosure into a superposition of nozzle-centric modes:

10   *A. K. Kushwaha, N. A. Worth, J. R. Dawson, V. Gupta and L. K. B. Li*

$$e^{iky} + e^{-iky} = \sum_{m=-\infty}^{\infty} C_m(kr)e^{im\theta} + \sum_{m=-\infty}^{\infty} C_m(kr)e^{-im\theta}, \tag{2.1}$$

$$= \sum_{m=-\infty}^{\infty} i^m J_m(kr)e^{im\theta} + \sum_{m=-\infty}^{\infty} (-i)^m J_m(kr)e^{-im\theta}, \tag{2.2}$$

where k and m are, respectively, the wavenumbers in the transverse (y) and azimuthal (θ) directions, r is the nozzle-centric radial coordinate, C_m is the modal amplitude, and J_m is the Bessel function of the first kind. For an acoustically compact nozzle ($kr \ll 1$), a Taylor-series expansion to leading order gives $J_m(kr) = (kr)^m/2^m m!$. Figure 3 shows that the acoustic disturbances generated at the pressure antinode (position $\mathbb{A}$) are dominated by the $m = 0$ mode, with no contribution from the $m = \pm 1$ modes (see inset), indicating pure axial forcing. Moving away from the pressure antinode (i.e. to positions $\mathbb{B} \to \mathbb{D}$), the $m = 0$ mode gradually weakens, while the $m = \pm 1$ modes gradually strengthen. These variations, however, are not symmetric in space: the $m = 0$ mode remains significantly stronger than the $m = \pm 1$ modes, even at positions $\mathbb{C}$ and $\mathbb{D}$. It is not until arriving fully at the pressure node (position $\mathbb{E}$) that the acoustic disturbances become dominated by the $m = \pm 1$ modes, with no contribution from the $m = 0$ mode, indicating pure transverse forcing. Crucially, for a given amplitude of the acoustic standing wave, the axial forcing ($m = 0$) produced at the pressure antinode (position $\mathbb{A}$) is more than an order of magnitude stronger than the transverse forcing ($m = \pm 1$) produced at the pressure node (position $\mathbb{E}$). Therefore, to provide representative comparisons between axial and transverse forcing, we adjust the amplitude of the acoustic standing wave such that the modal amplitude is kept constant across all five nozzle positions.

3. Low-dimensional model

One of the simplest low-dimensional models with self-excited temporal solutions is the VDP oscillator (van der Pol 1926). This model has been used throughout science and engineering to study various nonlinear phenomena (Pikovsky *et al.* 2003; Balanov *et al.* 2009), such as the frictional dynamics of tectonic plates (Cartwright *et al.* 1999), the interaction between vocal folds (Lucero & Schoentgen 2013), and thermoacoustic instabilities in combustors (Noiray & Schuermans 2013*a*; Guan *et al.* 2019*a*,*b*, 2021). Similarly, the forced VDP oscillator has been shown to be able to phenomenologically capture the forced synchronization dynamics of various globally unstable flows, such as cylinder wakes (Baek & Sung 2000), jet diffusion flames (Li & Juniper 2013*b*), and low-density jets (Li & Juniper 2013*a*,*c*).

However, the classic VDP oscillator contains only a single natural mode, whereas the present study concerns the interactions between axisymmetric and transverse hydrodynamic modes. Therefore, we use two coupled VDP oscillators, each forced externally by a sinusoidal term, to phenomenologically model the forced synchronization of the jet:

$$\ddot{x}_1 - \sigma_1 \dot{x}_1 + \omega_1^2 x_1 + \beta_1 x_1^2 \dot{x}_1 + \alpha_{12} x_2^2 \dot{x}_1 + \kappa_{12}(x_1 - x_2) = b_1 \sin(\omega_f t), \tag{3.1}$$

$$\ddot{x}_2 - \sigma_2 \dot{x}_2 + \omega_2^2 x_2 + \beta_2 x_2^2 \dot{x}_2 + \alpha_{21} x_1^2 \dot{x}_2 + \kappa_{21}(x_2 - x_1) = b_2 \sin(\omega_f t), \tag{3.2}$$

where x_1 is the dynamical variable of the oscillator (3.1) representing the axisymmetric mode ($m = 0$), and x_2 is the dynamical variable of the oscillator (3.2) representing the transverse mode ($m = \pm 1$). Linear growth is controlled by σ_1 and σ_2, nonlinear saturation is controlled by β_1 and β_2, and the natural angular frequencies in the linear limit are given by

Rapids articles must not exceed this page length

Quenching of a globally unstable jet via axisymmetry breaking   11

ω_1 and ω_2. Each oscillator is forced sinusoidally with an independent amplitude (b_1 or b_2) but at a common frequency (ω_f). Axial forcing is modelled by exciting the $m = 0$ oscillator (3.1: $b_1 > 0$), while transverse forcing is modelled by exciting the $m = \pm 1$ oscillator (3.2: $b_2 > 0$). Although our aim is to phenomenologically model the experimentally observed jet dynamics, care must be taken when choosing the values of the coefficients in both (3.1) and (3.2). For the $m = 0$ oscillator (3.1), we set $\sigma_1 = 0.07$ as per Lee *et al.* (2019), who used the Fokker–Planck equation to perform system identification of a low-density jet similar to the one studied here. We set $\beta_1 = 4$ because this produces a self-excited oscillation waveform that matches that found in our jet experiments. For the $m = \pm 1$ oscillator (3.2), we allow it to be globally stable ($\sigma_2 = -0.15$; $\beta_2 = 4$), in accordance with the stability analyses of Monkewitz & Sohn (1988), Jendoubi & Strykowski (1994), Lesshafft & Huerre (2007) and Coenen *et al.* (2008). The behaviour of the model remains qualitatively unchanged so long as σ_2 remains small and negative ($-0.18 < \sigma_2 < -0.01$). However, when b_2 increases, the amplitude of the $m = \pm 1$ oscillator also increases, causing it to compete with the $m = 0$ oscillator. We let $\omega_1 = 1$ and $\omega_2 = 1.04$, which is consistent with the analysis of Monkewitz & Sohn (1988) showing that the Strouhal number of the axisymmetric mode is slightly lower than that of the first helical mode. We use symmetric nonlinear coupling ($\alpha_{12} = \alpha_{21} = 3.6$) to model the stabilizing effect of base flow modifications induced by the growth of either of the two modes (Sipp & Lebedev 2007). We use symmetric linear reactive coupling ($\kappa_{12} = \kappa_{21} = 0.015$) to model mode competition (Balanov *et al.* 2009). We solve the coupled oscillator model (3.1 and 3.2) numerically for a wide range of forcing conditions (b_1, b_2, ω_f) in order to reproduce the synchronization phenomena observed in the jet experiments.

4. Natural jet dynamics

Before examining the forced jet response, it is important to identify a suitable operating point at which to apply external forcing. Figure 4 shows the amplitude and PSD of the HWA velocity fluctuations in the unforced jet over a range of *Re*. In this bifurcation diagram, we increase and decrease *Re* so as to test for hysteresis and bistability. We define the jet amplitude as the root-mean-square velocity fluctuation normalized by the time-averaged velocity: $\gamma'_{rms}/\overline{\gamma}$. By examining both the jet amplitude and PSD (figure 4), we find four distinct flow regimes.

(i) In regime I ($148 < Re < 400$), the jet is globally stable but convectively unstable, as evidenced by the low amplitude of its oscillations and by the absence of sharp peaks in the PSD. Physically, this implies that the amplification of background disturbances by local convective modes is not strong enough to overcome the stabilising influence of viscosity.

(ii) In regime II ($400 < Re < 562$), the jet is hysteretic: along the forward path (increasing *Re*), the jet amplitude is initially low but then jumps when *Re* reaches a critical value ($Re = 474$), coinciding with the emergence of a sharp peak in the PSD. This indicates an abrupt transition from a globally stable state (a fixed point) to a globally unstable state (a limit cycle) (Huerre & Monkewitz 1990). These limit-cycle oscillations are sustained by a balance between dissipation and extraction of energy, the latter from the base flow via the baroclinic torque (Lesshafft & Huerre 2007). Along the backward path (decreasing *Re*), the jet remains globally unstable throughout the entire regime; the PSD shown in figure 4(b) is for the forward path only. These differences between the forward and backward paths are characteristic of a subcritical Hopf bifurcation (Strogatz 1994). Subcritical Hopf bifurcations can arise in various flow systems (e.g. plane Poiseuille flow, Taylor–Couette flow, a Rijke tube; Reynolds & Potter 1967; Marques & Lopez 2006; Rigas *et al.* 2016), but they have only recently been discovered in low-density inertial jets (Zhu *et al.* 2017, 2019).

(iii) In regime III ($562 < Re < 695$), the jet amplitude increases sharply and then decreases with increasing *Re*, while the dominant frequency in the PSD remains roughly constant. This
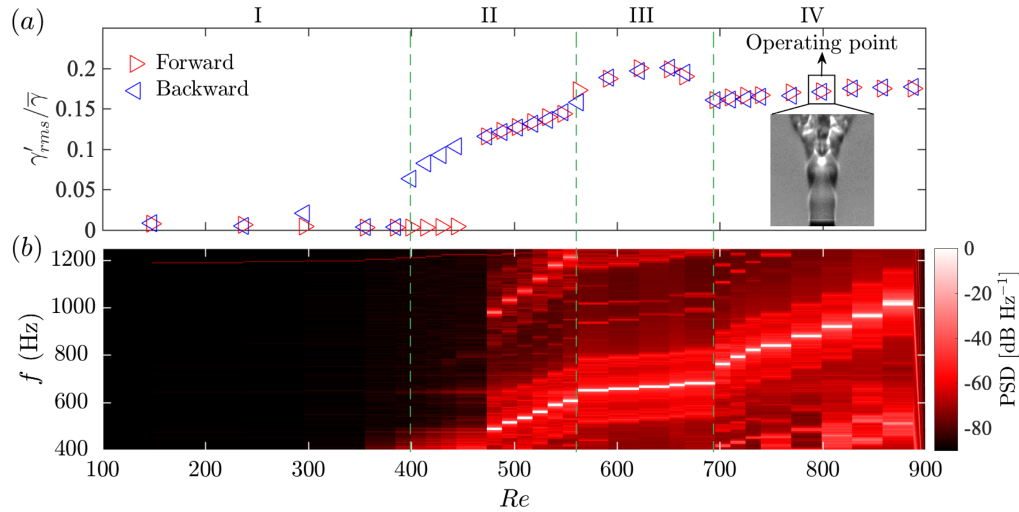
Figure 4: (a) Normalized amplitude and (b) PSD of the HWA velocity fluctuations in the unforced jet over a range of Re. Panel (b) is for the forward path only. In our forced synchronization tests (§5), we consider an operating point (regime IV: $Re = 800$) at which the jet is dominated by global hydrodynamic instability. The resultant self-excited oscillations are axisymmetric ($m = 0$), as shown in the schlieren snapshot (see inset).

indicates that the global hydrodynamic mode of the jet has locked into a natural acoustic mode of the nozzle, resulting in hydro-acoustic resonance at a constant Helmholtz number. This regime is to be avoided in our forced synchronization tests because the natural jet dynamics is no longer prescribed by global hydrodynamic instability.

(iv) In regime IV ($695 < Re < 888$), both the jet amplitude and frequency resume the upward trends that began in regime II, indicating that the global hydrodynamic mode is no longer locked into a natural acoustic mode of the nozzle. In regimes II and IV, the dominant frequency increases with Re in accordance with the scaling proposed by Hallberg & Strykowski (2006) based on a viscous diffusion time scale. This confirms that the instability is caused by hydrodynamic mechanisms alone, rather than by hydro-acoustic coupling.

In our forced synchronization tests (§5), we consider an operating point in regime IV where $Re = 800$ ($\pm 3.7\%$). We choose this particular point because it is far from regime II where hysteretic bistability occurs. It is also sufficiently far from regime III that, even at high forcing amplitudes, the instantaneous Re remains high enough to keep the jet in a purely hydrodynamically self-excited state, without the risk of it locking into the nozzle acoustics. Moreover, the Mach number ($M \equiv U_j/c_j = 1.6 \times 10^{-2}$, where c_j is the speed of sound) and the Richardson number ($Ri \equiv gD(\rho_\infty - \rho_j)/\rho_j U_j^2 = 1.3 \times 10^{-3}$) are both low enough to render the effects of compressibility and buoyancy insignificant. Finally, spatiotemporal stability analyses have shown that if the shear layers of a low-density axisymmetric jet are excessively thick, the helical modes ($m = \pm 1$) can join the axisymmetric mode ($m = 0$) in becoming locally absolutely unstable (Monkewitz & Sohn 1988; Jendoubi & Strykowski 1994; Lesshafft & Huerre 2007; Coenen *et al.* 2008). To prevent this, we ensure that the transverse curvature ($D/\theta_0 = 33.2$) at our chosen operating point ($Re = 800$) is in a range where local absolute instability exists in only the axisymmetric mode, and not in any of the helical modes (Jendoubi & Strykowski 1994). Consequently, the unforced jet is dominated by global hydrodynamic oscillations whose spatial mode structure is axisymmetric ($m = 0$), as shown in the schlieren snapshot of figure 4 (see inset).

5. Forced jet response

Having identified a suitable operating point (§4), we proceed to explore the forced synchronization of the jet. We apply time-periodic acoustic forcing of different amplitudes, frequencies ($0.8 < f_f/f_n < 1.2$), and symmetries (axial, transverse, and a mix of both). At each f_f, we incrementally increase the forcing amplitude to a value above that required for lock-in. We define the forcing amplitude as $a \equiv (a_1^2 + a_2^2)^{1/2}$, where a_1 is the maximum pressure oscillation amplitude at the nozzle outlet centreline and is a measure of the axial forcing amplitude, while a_2 is the maximum pressure gradient across the nozzle centreline and is a measure of the transverse forcing amplitude. We define the normalized response amplitude of the jet as $\eta_\gamma \equiv \gamma_{rms}'^* / \gamma_{rms}'$, where $\gamma_{rms}'^*$ and γ_{rms}' denote the root-mean-square HWA velocity fluctuations in the forced and unforced jets, respectively. The HWA data will be supplemented by PIV data in §5.2.

5.1. *Synchronization maps*

To provide an overview of the amplitude response and lock-in boundaries, we show in figure 5 the synchronization maps for the five jet positions examined in figure 3. These maps contain surfaces of η_γ in a parameter space defined by a and f_f/f_n. The red and blue regions correspond, respectively, to amplification and attenuation of the self-excited jet oscillations. For each value of f_f/f_n, the minimum value of a required for lock-in, a_{loc}, is indicated by circular markers. As noted in §1.2, the region above these markers is known as the 1:1 Arnold tongue (Balanov *et al.* 2009). The filled (black) markers denote a saddle-node bifurcation along the phase-locking route to lock-in, whereas the hollow (white) markers denote an inverse Neimark–Sacker bifurcation along the suppression route to lock-in; these two routes will be examined in §5.3.1 and §5.3.2. In this study, we define lock-in as a completely synchronous state in which the instantaneous phase difference between the forcing signal and the forced self-excited system is constant in time; this state is known as phase locking in the synchronization literature and can be reached via either the phase-locking or suppression route (Pikovsky *et al.* 2003). Prior to lock-in ($a < a_{loc}$), the jet is either partially synchronized (phase trapping) or desynchronized (phase drifting), depending on its proximity to the Arnold tongue; these intermediate quasiperiodic states will also be examined in §5.3.1 and §5.3.2.

The synchronization maps in figure 5 reveal that a_{loc} increases as f_f/f_n deviates from 1, producing a classic ∨-shaped Arnold tongue centred on the natural mode ($f_f/f_n = 1$). The shape and position of the Arnold tongue remain similar across all five jet positions, indicating that the jet always locks in at the same set of forcing amplitudes regardless of the symmetry of the imposed perturbations, i.e. regardless of whether the forcing is purely axial (position $\mathbb{A}$), purely transverse (position $\mathbb{E}$), or a mix of the two (positions $\mathbb{B}$, $\mathbb{C}$, and $\mathbb{D}$).

An examination of the η_γ surfaces shows that when the jet is forced purely axially (figure 5: position $\mathbb{A}$), its oscillations within the Arnold tongue are amplified when $f_f/f_n < 1$ (red regions) but are attenuated when $f_f/f_n > 1$ (blue regions). This is consistent with the experiments by Li & Juniper (2013*a*), who found the same asymmetry in a similar jet subjected to pure axial forcing from a loudspeaker mounted upstream of the nozzle outlet. In figure 5, the asymmetry in η_γ also appears at all the jet positions between the pressure antinode and node (positions $\mathbb{B}$, $\mathbb{C}$, and $\mathbb{D}$). This is not surprising given that the acoustic perturbations at these intermediate jet positions are still dominated by the axial mode (figure 3), just as they are at the pressure antinode itself (figure 5: position $\mathbb{A}$). As §5.4 will show, the asymmetry in η_γ is caused by non-resonant amplification of the forcing signal when $f_f/f_n < 1$.

When the jet is forced purely transversely (figure 5: position $\mathbb{E}$), its oscillations become suppressed across the full range of f_f/f_n. Crucially, this suppression occurs not just inside the Arnold tongue but also outside it, demonstrating the robustness of this control technique

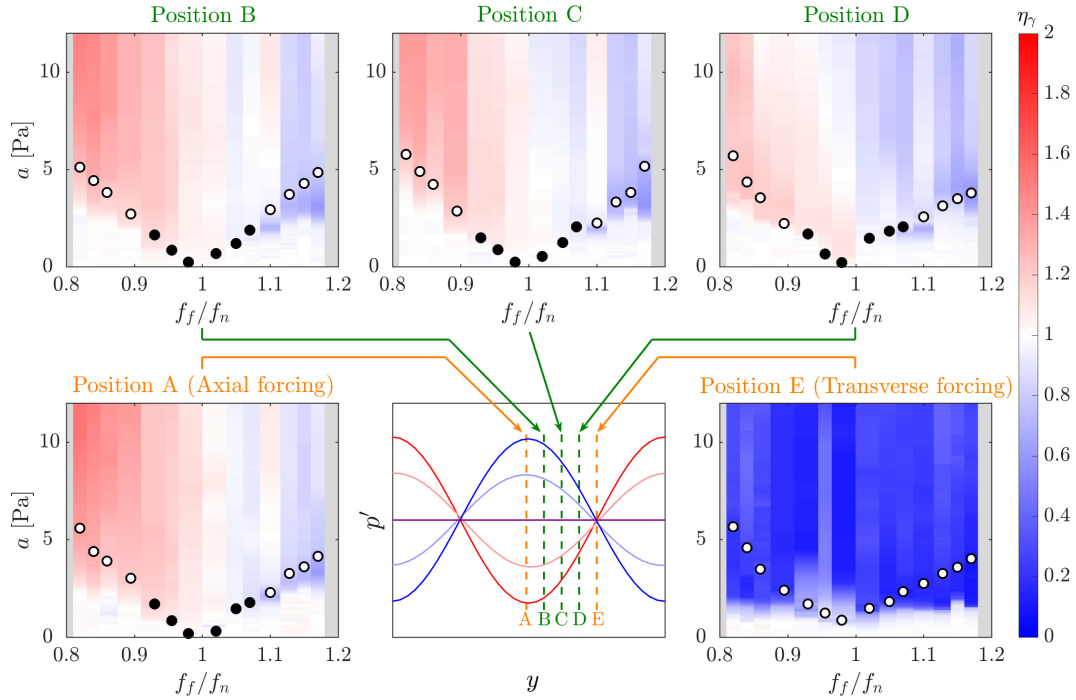14   *A. K. Kushwaha, N. A. Worth, J. R. Dawson, V. Gupta and L. K. B. Li*

Figure 5: Synchronization maps from the forced jet experiments. The surface colours denote the normalized response amplitude ($\eta_\gamma \equiv \gamma'^*_{rms}/\gamma'_{rms}$), shown in a parameter space defined by the forcing amplitude (a) and the normalized forcing frequency (f_f/f_n). The minimum value of a required for lock-in, a_{loc}, is indicated by circular markers, which form the lower boundaries of the 1:1 Arnold tongue. The filled (black) markers denote a saddle-node bifurcation along the phase-locking route to lock-in, whereas the hollow (white) markers denote an inverse Neimark–Sacker bifurcation along the suppression route to lock-in.
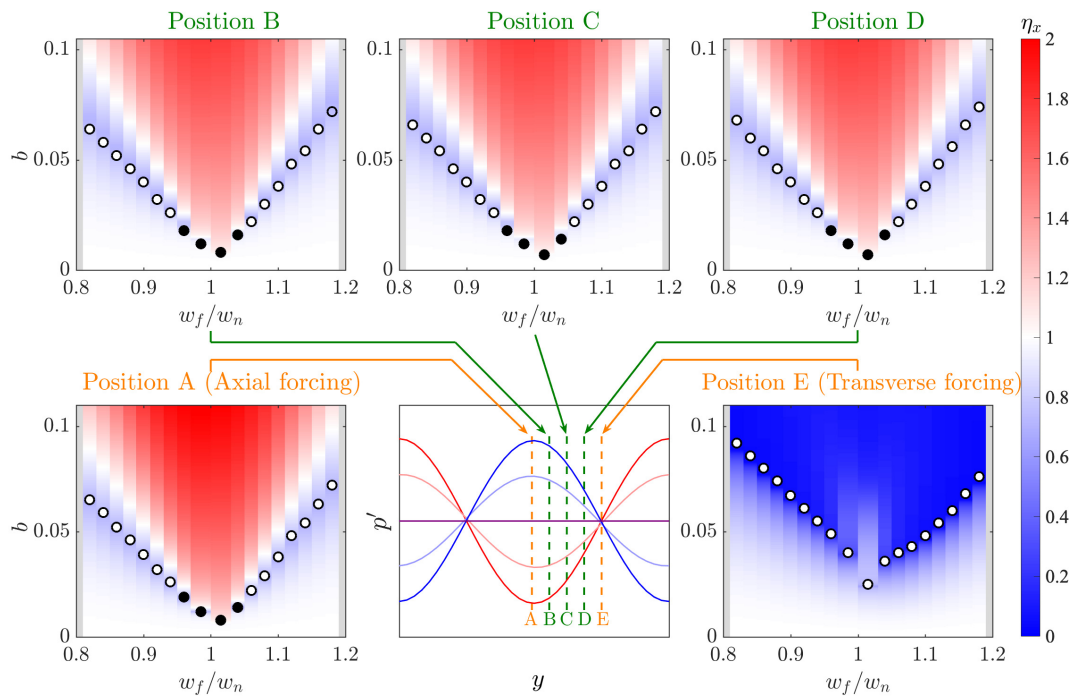
Figure 6: The same as for figure 5 but from the forced VDP model (3.1 and 3.2).

(i.e. axisymmetry breaking) to variations in both f_f and a. The degree of suppression is generally high: the oscillation amplitude can be reduced to less than 10–15% of that of the unforced jet in most of the parameter space (figure 5: position $\mathbb{E}$). As §5.4 will show, this suppression of the self-excited jet oscillations occurs via asynchronous and synchronous quenching, both without any amplification of the forcing signal.

We have shown from a synchronization perspective that breaking the axisymmetry of a globally unstable jet via transverse forcing can lead to a more effective means of open-loop flow control than preserving the axisymmetry via axial forcing. In particular, although the shape and position of the Arnold tongue (a_{loc}) are relatively insensitive to the symmetry of the imposed perturbations, the jet oscillations themselves are suppressed more readily with transverse forcing than with axial forcing. Compared with pure axial forcing (position $\mathbb{A}$) and axially dominated forcing (positions $\mathbb{B}$, $\mathbb{C}$, and $\mathbb{D}$), pure transverse forcing (position $\mathbb{E}$) can produce larger reductions in η_γ with fewer limitations on the required values of f_f and a. By contrast, when $f_f/f_n < 1$, axial forcing, even when combined with transverse forcing, can cause η_γ to exceed unity. This amplification occurs because the axisymmetric global mode ($m = 0$) is preferentially receptive to perturbations matching its own spatial structure, a phenomenon that will be examined further in §5.4.

The synchronization maps for the model are shown in figure 6. As before, the surface colours denote the normalized response amplitude ($\eta_x \equiv x'^*_{rms}/x'_{rms}$), and the circular markers denote the onset of lock-in via a saddle-node bifurcation (filled black markers) or an inverse Neimark–Sacker bifurcation (hollow white markers). The forcing amplitude is defined as $b \equiv (b_1^2 + b_2^2)^{1/2}$, with the minimum value of b required for lock-in denoted by b_{loc}. Comparing figures 5 and 6, we find many similarities but also some key differences between the jet and the model. In both systems, the minimum forcing amplitude required for lock-in (a_{loc}, b_{loc}) increases with detuning regardless of the symmetry of the imposed perturbations, resulting in a familiar $\vee$-shaped Arnold tongue centred on the natural mode ($f_f/f_n = 1$, $\omega_f/\omega_n = 1$). Furthermore, when forced purely transversely (figures 5 and 6: position $\mathbb{E}$), the self-excited oscillations in both systems become readily suppressed across a wide range of forcing frequencies and amplitudes, highlighting again the effectiveness of axisymmetry breaking as a quenching strategy. However, a notable feature of the jet that could not be captured by the model is the asymmetry in η_γ about $f_f/f_n = 1$, which occurs whenever the imposed perturbations are axially dominated, i.e. at positions $\mathbb{A}$ to $\mathbb{D}$ in figure 5. This discrepancy was also noted by Li & Juniper (2013a) but its origin has yet to be fully established. Nevertheless, it is encouraging to see how such a simple model can still accurately, albeit qualitatively, capture the extensive amplitude suppression observed in the purely transversely forced jet, including its insensitivity to both f_f and a (figures 5 and 6: position $\mathbb{E}$).

5.2. *Amplitude suppression and symmetry breaking of the wavemaker region*

The extensive amplitude suppression observed in the purely transversely forced jet (figure 5) was established based on local measurements made with a spatially fixed HWA probe. To verify that the observed suppression is not simply an artefact of the nonlinear global mode shifting away from the HWA probe, we show in figure 7(a–c) the spatial distribution of the total velocity fluctuation (i.e. the root mean square of V', or V'_{rms}), as measured with stereoscopic time-resolved PIV, for both axial and transverse forcing as well as for no forcing at all. Our focus is on the potential core, rather than on the regions downstream, because that is where the wavemaker of the global mode is known to reside (Lesshafft *et al.* 2006; Qadri *et al.* 2018). We demarcate the potential core with a black line representing the regions

16   *A. K. Kushwaha, N. A. Worth, J. R. Dawson, V. Gupta and L. K. B. Li*

where $\overline{V}$ exceeds 95% of its value at the nozzle outlet centreline. In figure 7(d–f), we show the normalized PSD of V' along the jet centreline ($y/D = 0$) at different axial stations.

When the jet is unforced (figure 7a), V'_{rms} increases from around zero at the nozzle outlet ($x/D \approx 0$) to a local maximum within the potential core ($x/D \approx 1.5$, coinciding with the HWA probe location; §2.1), before eventually decreasing downstream towards the tip. The corresponding PSD (figure 7d) shows that these self-excited oscillations occur at the fundamental frequency of the natural global mode (f_n). Farther downstream ($x/D > 2.3$), the subharmonic ($f_n/2$) overtakes the fundamental (f_n) to become the new dominant mode. This coincides with regions of large V'_{rms} outside the potential core. Such strong $f_n/2$ oscillations in the downstream region are known to arise from period doubling associated with vortex pairing, possibly aided by disturbance amplification from local convective modes (Kyle & Sreenivasan 1993). From these observations, we can conclude that the potential core of the jet is dominated by a global hydrodynamic mode at its natural fundamental frequency (f_n).

When the jet is forced purely axially at a_{loc} and $f_f/f_n = 1.09$ (figure 7b), V'_{rms} becomes lower than that of the unforced jet, particularly in the potential core, which is now noticeably shorter. This amplitude reduction for $f_f > f_n$ is consistent with the η_γ data (figure 5) extracted from our local HWA measurements. The corresponding PSD (figure 7e) shows that, as is the case without forcing, most of the potential core oscillates at the fundamental frequency of the dominant mode, which is now at f_f (not f_n) because the jet has locked into the forcing. For a similar reason, the regions downstream oscillate at the subharmonic of the forced mode ($f_f/2$), rather than at the subharmonic of the natural global mode ($f_n/2$).

When the jet is forced purely transversely at a_{loc} and $f_f/f_n = 1.09$ (figure 7c), V'_{rms} becomes even lower than that of the purely axially forced jet (figure 7b), with most of the decrease occurring in the potential core. Also decreasing is the streamwise extent of the potential core itself, although most of its spatial domain ($x/D < 2$) remains dominated by the f_f mode, with the regions downstream dominated by the $f_f/2$ mode (figure 7f). Crucially, the fact that regardless of whether the forcing is axial (figure 7b) or transverse (figure 7c), the decrease in V'_{rms} occurs spatially throughout most of the potential core, where the wavemaker is known to reside (Lesshafft *et al.* 2006; Qadri *et al.* 2018), confirms that our single-point HWA measurements are indeed a reliable indicator of the jet response.

To assess the symmetry of the vortical structures in the jet, we show in figure 7(g–i) the dominant spatial modes extracted via dynamic mode decomposition (DMD, Schmid 2010; Rowley & Dawson 2017) of the in-plane velocity field (u, v) measured with PIV. These DMD modes are dominant in the sense that their amplitudes are the highest in their respective spectra; they correspond to the f_n mode in the unforced jet (figure 7g) and to the f_f mode in both the purely axially forced jet (figure 7h) and the purely transversely forced jet (figure 7i). Superimposed over the DMD modes are contours of the out-of-plane vorticity fluctuation. In all three cases (figure 7g–i), the jet dynamics are periodic, either naturally or due to lock-in, with each DMD mode featuring a train of counter-rotating vortical structures advecting along the shear layers on both sides of the jet centreline.

In both the unforced jet (figure 7g) and the purely axially forced jet (figure 7h), the vortical structures are antisymmetric about the jet centreline, which is consistent with the presence of an $m = 0$ global mode. To quantify the phase shift between the left and right shear layers (Θ), we apply the Hilbert transform to instantaneous streamwise profiles of vorticity extracted at $y/D = \pm 0.5$, and then plot the data in figure 7(j) as a normalized histogram of Θ. We find that the histogram peaks at $\Theta \approx 0$ for both the unforced and axially forced jets, confirming that the left and right shear layers are rolling up in-phase with each other. This is the classic behaviour of an axisymmetric jet dominated by an $m = 0$ global mode.

In the purely transversely forced jet (figure 7i), however, the vortical structures are no longer antisymmetric about the jet centreline. Instead, they roll up and advect out-of-phase

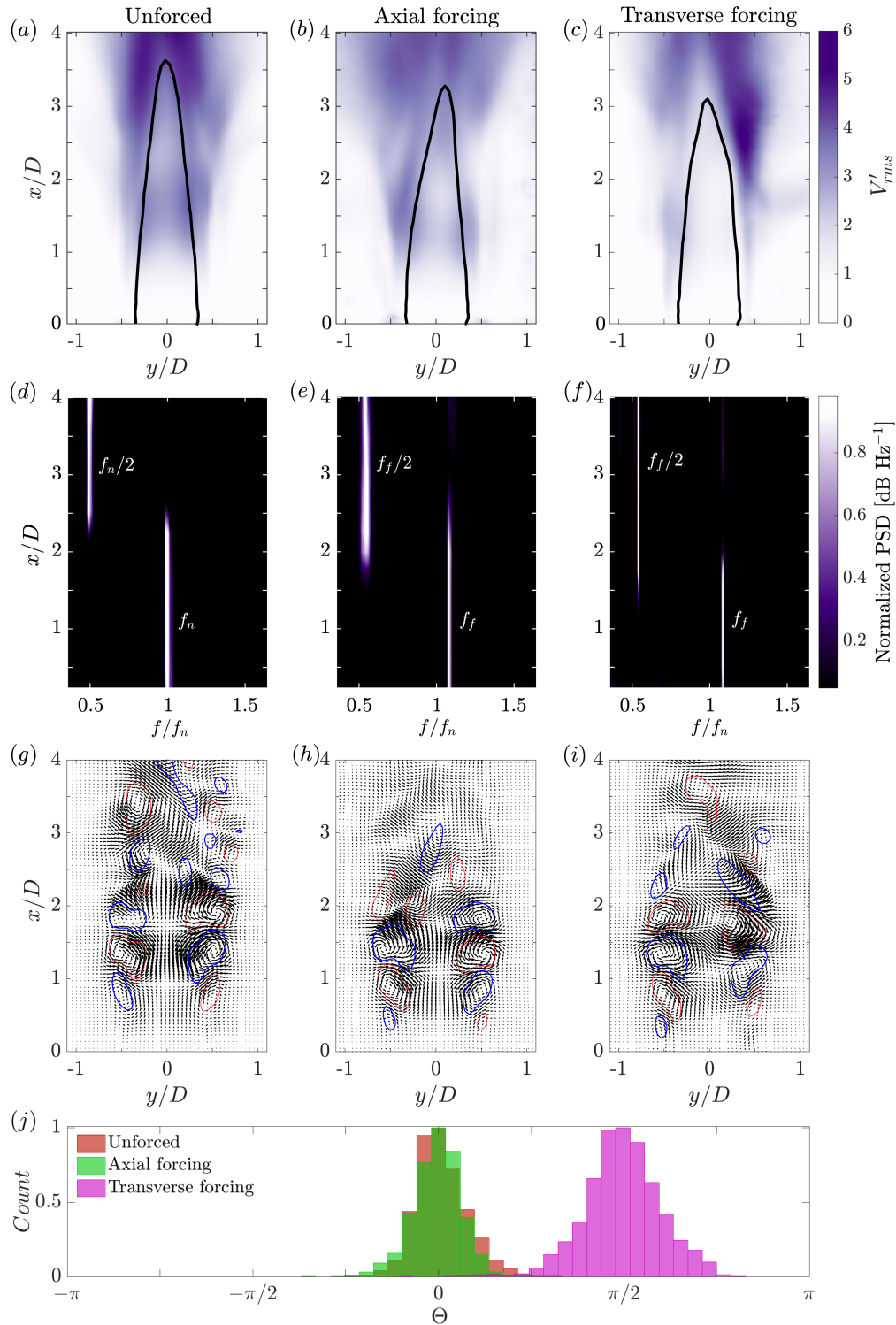*Quenching of a globally unstable jet via axisymmetry breaking*   17

Figure 7: Spatial distribution of the forced jet response, as measured with stereoscopic time-resolved PIV: (a–c) the root mean square of the total velocity fluctuation V'_{rms}, (d–f) the normalized PSD of V' along the jet centreline ($y/D = 0$), (g–i) the dominant DMD mode with contours of the out-of-plane vorticity fluctuation, and (j) the normalized histogram of the phase shift Θ between the left and right shear layers. Three representative forcing conditions are shown: (left) unforced, (middle) pure axial forcing at a_{loc}, and (right) pure transverse forcing at a_{loc}. With either axial or transverse forcing, the forcing frequency is fixed at $f_f/f_n = 1.09$.

by $\pi/2$ (figure 7j), producing a transverse flapping motion that breaks the axisymmetry of the $m = 0$ global mode. Put together, these findings provide compelling evidence that axial forcing preserves the inherent axisymmetry of the jet, whereas transverse forcing breaks that axisymmetry by inducing the staggered roll-up of vortical structures in the shear layers. The latter effect will prove to be crucial in achieving asynchronous and synchronous quenching of the natural global mode, without amplification of the forced mode.

5.3. *Bifurcation routes to lock-in*

Having examined the spatial characteristics of the forced jet response, we now turn to identifying the bifurcations responsible for lock-in. We first consider the purely axially forced jet (§5.3.1: position $\mathbb{A}$) so as to establish a calibrated baseline against the axial forcing experiments of Li & Juniper (2013*a*,*c*). We then compare this to the purely transversely forced jet (§5.3.2: position $\mathbb{E}$) so as to determine the effects of axisymmetry breaking. In the interest of brevity, we do not show results for combined axial–transverse forcing (positions $\mathbb{B}$, $\mathbb{C}$, and $\mathbb{D}$) because they are qualitatively similar to those for pure axial forcing (position $\mathbb{A}$). This is expected because all four of these jet positions (positions $\mathbb{A}$, $\mathbb{B}$, $\mathbb{C}$, and $\mathbb{D}$) are dominated by axial perturbations ($m = 0$), with little to no contribution from transverse perturbations ($m = \pm 1$), as was shown in figure 3. For each type of forcing, we consider two representative values of f_f, one close to f_n and one far from f_n. This is so that we can investigate the full range of synchronization dynamics around the 1:1 Arnold tongue.

5.3.1. *Axial forcing: the jet at position $\mathbb{A}$*

Figure 8 shows the synchronization dynamics of the jet when forced axially at a frequency close to its natural global frequency: $f_f/f_n = 1.04$. We consider the (a) time trace, (b) PSD, (c) instantaneous phase difference between the forcing signal and the forced self-excited jet, $\Delta\phi_{f,\gamma}$, and (d) one-sided Poincaré map, all extracted from the $\gamma(t)$ signal. For comparison, we show in figure 9 the same indicators but for the axially forced model. In both systems, we incrementally increase the forcing amplitude until reaching the onset of lock-in, which occurs at $A \equiv a/a_{loc} = 1$ for the jet and at $B \equiv b/b_{loc} = 1$ for the model.

When unforced (figure 8: $A = 0$), the jet is hydrodynamically self-excited, exhibiting a nonlinear global mode at f_n with progressively weaker components at the subharmonic and superharmonics (both odd and even; figure 8a,b). In the absence of forcing, $\Delta\phi_{f,\gamma}$ is undefined, so we plot in figure 8(c: bottom row) the instantaneous phase evolution of the unforced jet, $-\phi_\gamma$, which is seen to drift continuously in time without phase slips. This behaviour is consistent with the absence of pronounced amplitude modulation in the time trace (figure 8a) (Pikovsky *et al.* 2003). In the Poincaré map (figure 8d), the intercepts of the phase trajectory are concentrated at a single spot, indicating the presence of a closed repetitive orbit in the phase portrait, a signature feature of a period-1 limit-cycle attractor.

When forced at intermediate amplitudes (figure 8: $A = 0.25$–0.93), the jet becomes quasiperiodic. This is evidenced by the appearance of amplitude modulation in the time trace (figure 8a) and by the emergence of sharp peaks at both the forced (f_f) and natural (f_n^*) modes in the PSD (figure 8b). The values of f_f and f_n^* are incommensurable and, through the action of nonlinear resonant 3-wave interactions (Schmid *et al.* 2002), they generate a train of spectral peaks at linear combinations of f_f and f_n^*. Quasiperiodicity is also demonstrated by $\Delta\phi_{f,\gamma}$ drifting unboundedly in time (figure 8c) and by the formation of a closed ring of trajectory intercepts in the Poincaré map (figure 8d). Taken together, these observations indicate that the jet has transitioned from a period-1 limit-cycle attractor to an ergodic two-dimensional torus attractor $\mathbb{T}^2$ via a Neimark–Sacker bifurcation at $A = 0 \rightarrow 0.25$ (Pikovsky *et al.* 2003; Balanov *et al.* 2009). Several other features are worth noting in this quasiperiodic regime. As A increases, the natural mode at f_n^* gradually shifts towards the forced mode at
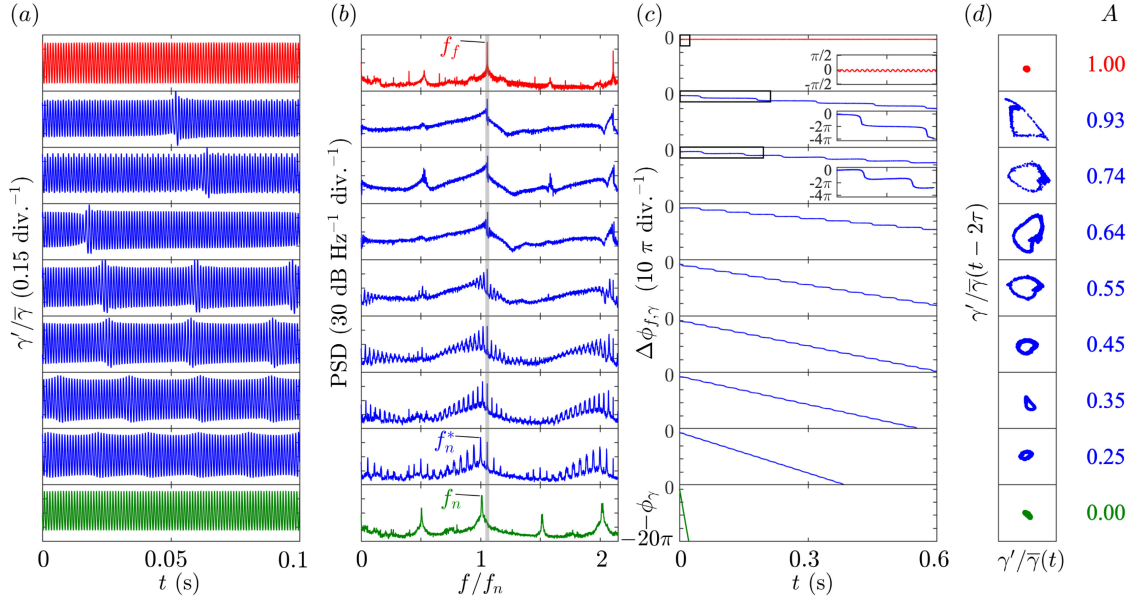
Figure 8: Synchronization dynamics of the jet when forced axially (position $\mathbb{A}$) at a frequency close to its natural global frequency: $f_f/f_n = 1.04$. The (a) time trace, (b) PSD, (c) temporal evolution of $\Delta\phi_{f,\gamma}$, and (d) one-sided Poincaré map are shown for nine forcing amplitudes, including the unforced case ($A = 0$). Lock-in occurs via the phase-locking route, which involves a Neimark–Sacker bifurcation at $A = 0 \rightarrow 0.25$ followed by a saddle-node bifurcation at $A = 0.93 \rightarrow 1$. The unforced state is shown in green, the quasiperiodic states are shown in blue, and the onset of lock-in is shown in red.
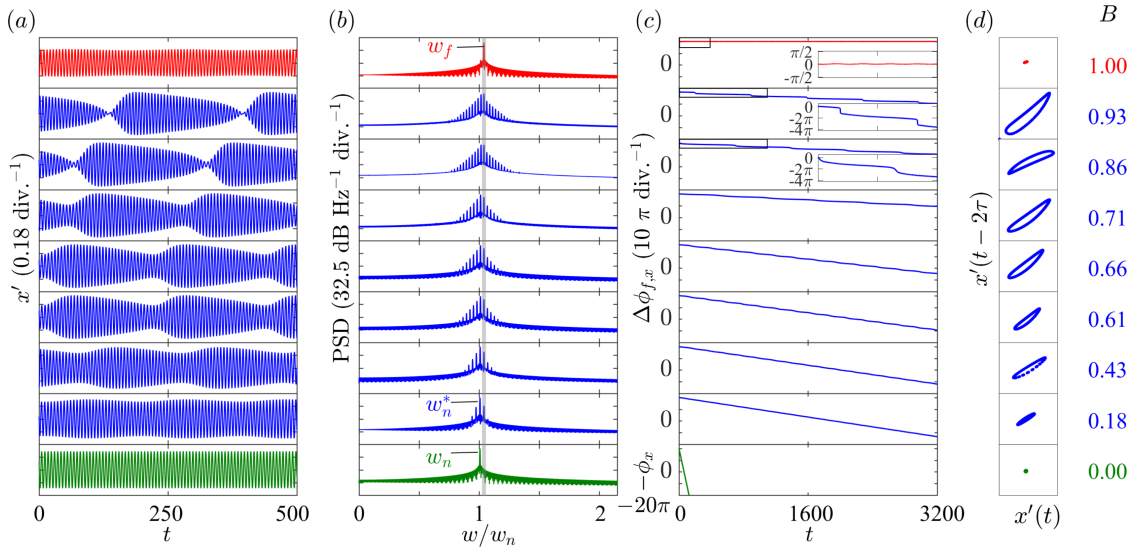
Figure 9: The same as in figure 8 but for the axially forced model at $\omega_f/\omega_n = 1.04$.

f_f, whose value is dictated by the external forcing and is thus fixed. This temporal adjustment process, known as frequency pulling in the synchronization literature, is a hallmark feature of the phase-locking route to lock-in (Pikovsky *et al.* 2003; Balanov *et al.* 2009). As for the phase difference (figure 8c), frequency pulling causes the time-averaged slope of $\Delta\phi_{f,\gamma}$, or $\langle\Delta\dot{\phi}_{f,\gamma}\rangle$, to approach zero gradually as A increases. Physically, this implies that the time scale of the natural mode is adjusting to match that of the forced mode. This process occurs without significant changes in the oscillation amplitude (figure 8a). Consequently, lock-in along the phase-locking route occurs via adjustments in the frequency rather than

in the amplitude, which is physically consistent with this route arising only when f_f is sufficiently close to f_n. Another notable feature is that at relatively high forcing amplitudes (figure 8c: $A = 0.74$–0.93), $\Delta\phi_{f,\gamma}$ drifts increasingly nonlinearly, spending long epochs at nearly constant values and then dropping abruptly by one complete cycle of 2π (see insets of figure 8c). In synchronization theory, the sudden loss or gain of an integer number of complete cycles is known as phase slipping and is another defining feature of the phase-locking route (Pikovsky *et al.* 2003). As A increases towards the value required for lock-in ($A = 1$), the time between successive phase slips increases. Physically, this implies that the jet is spending more and more time oscillating at f_f, with fewer phase slips. Meanwhile, the Poincaré map shows that the phase trajectory continues to wrap around the ergodic $\mathbb{T}^2$ torus attractor, whose scale grows monotonically as A increases (figure 8d). This confirms that the jet is still oscillating quasiperiodically at two incommensurable frequencies.

When forced at a critical amplitude (figure 8: $A = 1$), the jet transitions from $\mathbb{T}^2$ quasiperiodicity to 1:1 lock-in: it now oscillates at only f_f and its harmonics, with no sign of the original natural mode at f_n^* (figure 8b). As a result, the time trace is no longer modulated (figure 8a), and $\Delta\phi_{f,\gamma}$ no longer drifts or slips but instead remains constant in time (figure 8c), indicating phase locking (Pikovsky *et al.* 2003). As expected, this transition from $\mathbb{T}^2$ quasiperiodicity to 1:1 lock-in sees the ring structure in the Poincaré map replaced by a single cluster of trajectory intercepts, indicative of a period-1 orbit (figure 8d). Crucially, the collapse of the ring structure occurs suddenly rather than gradually (figure 8d: $A = 0.93 \rightarrow 1$). According to synchronization analyses of the forced VDP oscillator (Balanov *et al.* 2009), the suddenness of this collapse indicates that the $\mathbb{T}^2$ attractor is still alive but has become resonant through a saddle-node bifurcation. Consequently, a pair of periodic orbits – one stable orbit and one saddle orbit – is born on the resonant $\mathbb{T}^2$ surface, with lock-in occurring when the phase trajectory snaps on to the stable orbit. This synchronization mechanism, involving a saddle-node bifurcation and frequency pulling, is intrinsic to the phase-locking route to lock-in (Balanov *et al.* 2009).

As mentioned earlier, figure 9 shows the same four indicators as figure 8 but for the axially forced model. We find that the model can qualitatively reproduce the main synchronization phenomena exhibited by the jet. These include (i) a Neimark–Sacker bifurcation from a period-1 limit cycle to $\mathbb{T}^2$ quasiperiodicity when axial forcing is first applied, (ii) amplitude modulation of the time trace, along with phase drifting and slipping during $\mathbb{T}^2$ quasiperiodicity, (iii) a gradual pulling of f_n^* towards f_f as the forcing amplitude increases, causing $\langle\Delta\dot\phi_{f,\gamma}\rangle$ to approach zero gradually, and (iv) a saddle-node bifurcation from $\mathbb{T}^2$ quasiperiodicity to 1:1 lock-in at a critically high forcing amplitude. However, the model cannot reproduce the train of spectral peaks observed at and around the subharmonic and superharmonics of f_n. This is because the VDP kernel used in the model contains only cubic nonlinearity, thus generating only odd harmonics (Nayfeh & Mook 1995). Although incorporating other forms of nonlinearity may improve the comparison, doing so is not a priority here. Our primary aim is to use the simplest possible model to phenomenologically capture the most salient synchronization phenomena of the jet, such as its Arnold tongue, bifurcation routes to lock-in, phase dynamics, and oscillation quenching mechanisms.

Next we increase f_f so that it is far from f_n (figure 10: $f_f/f_n = 1.17$). We find several important differences relative to the earlier case where f_f is close to f_n (figure 8: $f_f/f_n = 1.04$). In particular, lock-in now occurs not through a gradual pulling of f_n^* towards f_f, but through a gradual reduction in the amplitude of the natural mode. This fundamental change in the synchronization mechanism can be seen in the PSD (figure 10b), where the frequency (f_n^*) of the spectral peak corresponding to the natural mode remains constant as A increases. The difference can also be seen in the temporal evolution of the phase difference (figure 10c),
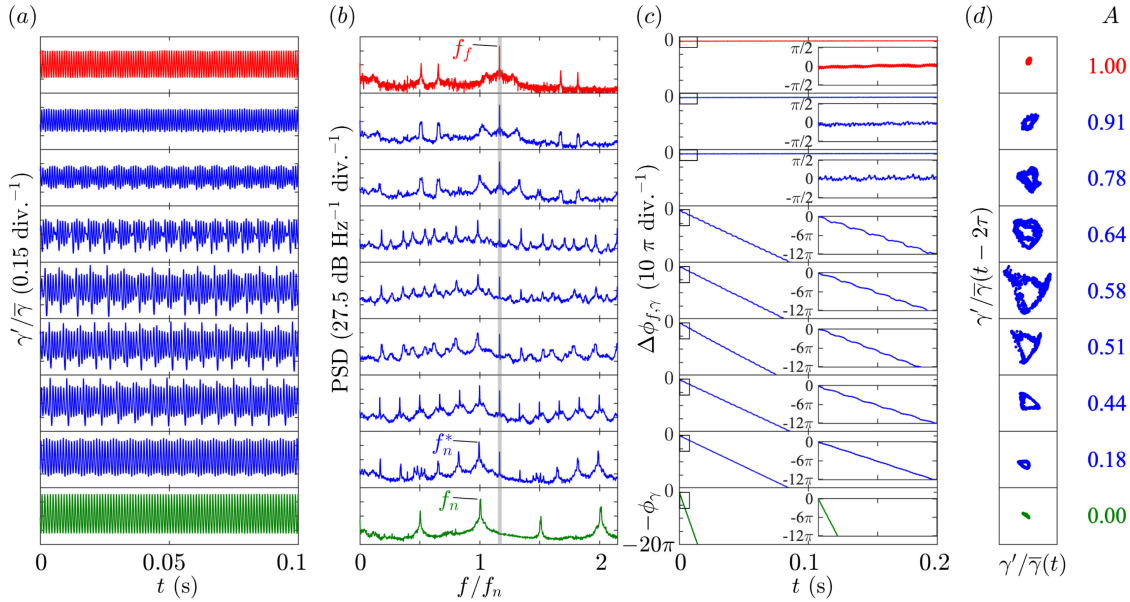
Figure 10: Synchronization dynamics of the jet when forced axially (position $\mathbb{A}$) at a frequency far from its natural global frequency: $f_f/f_n = 1.17$. The (a) time trace, (b) PSD, (c) temporal evolution of $\Delta\phi_{f,\gamma}$, and (d) one-sided Poincaré map are shown for nine forcing amplitudes, including the unforced case ($A = 0$). Lock-in occurs via the suppression route, which involves a Neimark–Sacker bifurcation at $A = 0 \to 0.18$ followed by an inverse Neimark–Sacker bifurcation at $A = 0.91 \to 1$. The unforced state is shown in green, the quasiperiodic states are shown in blue, and the onset of lock-in is shown in red.
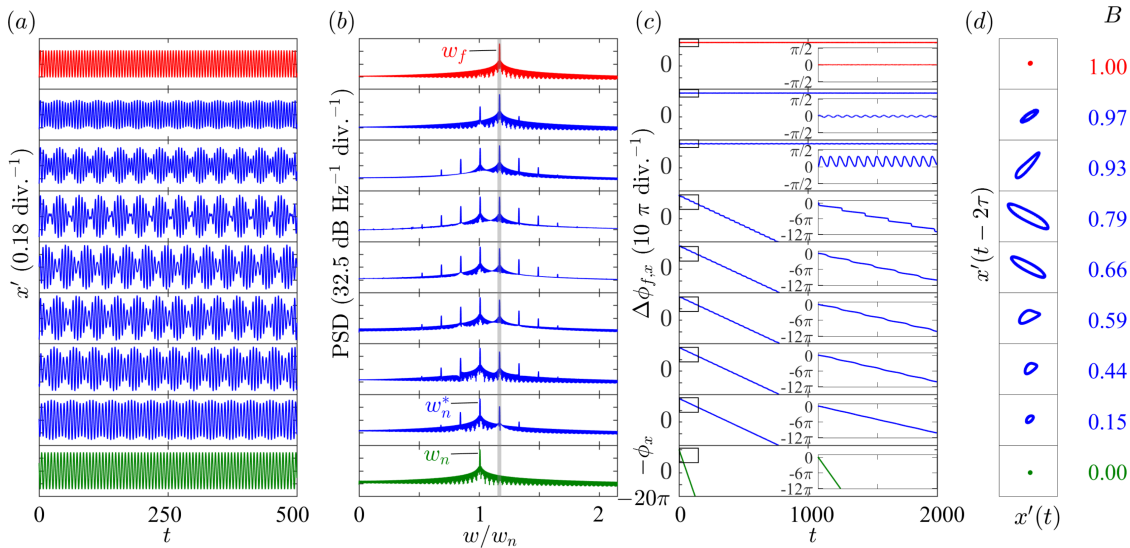

Figure 11: The same as in figure 10 but for the axially forced model at $\omega_f/\omega_n = 1.17$.

where $\langle\Delta\dot\phi_{f,\gamma}\rangle$ remains constant as A increases, until it eventually snaps to zero at the onset of phase trapping ($A = 0.78$) (Aronson *et al.* 1990; Thévenin *et al.* 2011).

As A increases from the onset of phase trapping, the ring structure in the Poincaré map shrinks gradually (figure 10d: $A = 0.78 \to 1$), indicating that the underlying $\mathbb{T}^2$ attractor is gradually collapsing to its death via an inverse Neimark–Sacker bifurcation (Balanov *et al.* 2009). This gradual collapse stands in stark contrast to the sudden collapse seen in figure 8(d), where the detuning is reduced. According to synchronization analyses of the forced VDP oscillator (Balanov *et al.* 2009), this difference is consistent with the jet locking into the

22   *A. K. Kushwaha, N. A. Worth, J. R. Dawson, V. Gupta and L. K. B. Li*

forcing via the suppression route, rather than the phase-locking route. In other words, instead of adjusting its phase dynamics (i.e. advancement or retardation of its temporal rhythm) to match that of the forcing, the jet experiences a suppression of its natural amplitude dynamics (Pikovsky *et al.* 2003). Because in this example f_f/f_n is sufficiently larger than 1, the suppression of the natural mode occurs without resonant amplification of the forced mode, resulting in the oscillation amplitude at lock-in (figure 10a: $A = 1$) being lower than that in the unforced state (figure 10a: $A = 0$). In synchronization theory, a suppression of the natural mode by non-resonant forcing is often referred to as asynchronous quenching (Bogoliubov & Mitropolsky 1961; Minorsky 1967, 1974), which will be examined further in §5.4.

For comparison, we show in figure 11 the same four indicators as figure 10 but for the axially forced model. As is the case when f_f is close to f_n (figures 8 and 9), we find that the model can qualitatively reproduce the main synchronization phenomena exhibited by the jet. Crucially, these include features specific to the suppression route to lock-in, such as (i) a gradual reduction in the amplitude of the natural mode as A increases, without a simultaneous pulling of f_n^* towards f_f, (ii) a constant value of $\langle \Delta \dot{\phi}_{f,\gamma} \rangle$ followed by an abrupt snap to zero at the onset of phase trapping, and (iii) a gradual reduction in the size of the ring structure in the Poincaré map, indicating an inverse Neimark–Sacker bifurcation from $\mathbb{T}^2$ quasiperiodicity to 1:1 lock-in at a critically high forcing amplitude.

In summary, we have investigated the forced synchronization of a prototypical hydrodynamic oscillator – a globally unstable low-density axisymmetric jet – located at the pressure antinode of a planar acoustic standing wave, where axial (symmetric, $m = 0$) perturbations were produced at different amplitudes and frequencies. We found that, around the 1:1 Arnold tongue, the jet exhibits a complex range of synchronization phenomena, such as (i) phase drifting, slipping and trapping during quasiperiodicity on a $\mathbb{T}^2$ attractor at intermediate A values, (ii) phase locking on a periodic orbit at critically high A values, and (iii) two bifurcation routes to lock-in: the phase-locking route when the detuning is small, and the suppression route when the detuning is large. We then showed that these synchronization phenomena could be qualitatively captured by the simple VDP model proposed in §3. These findings are broadly consistent with the experiments conducted by Li & Juniper (2013a,c) on a similar hydrodynamically self-excited jet forced axially from upstream with a loudspeaker mounted in the nozzle plenum. This further validates the present experimental methodology and data analysis, paving the way for an exploration of the effects of axisymmetry breaking via transverse forcing.

5.3.2. *Transverse forcing: the jet at position* $\mathbb{E}$

Figure 12 shows the synchronization dynamics of the jet when forced transversely at a frequency close to its natural global frequency: $f_f/f_n = 1.04$. Comparing this with figure 8, we find that switching from axial to transverse forcing at small detuning leads to a dramatic change in the jet response. In particular, although the jet still transitions from unforced periodicity to $\mathbb{T}^2$ quasiperiodicity via a Neimark–Sacker bifurcation when forcing is first applied (figure 12: $A = 0 \rightarrow 0.14$), the subsequent transition to 1:1 lock-in no longer occurs via a saddle-node bifurcation, as would be expected from figure 8 and from weakly nonlinear analyses of the classic (single-mode) VDP model when f_f is close to f_n (Pikovsky *et al.* 2003; Balanov *et al.* 2009). Instead, we find in figure 12 that, as A increases in the quasiperiodic regime, the frequency (f_n^*) of the natural mode remains constant but its amplitude decreases gradually, indicating asynchronous quenching without frequency pulling. In turn, this causes $\langle \Delta \dot{\phi}_{f,\gamma} \rangle$ to remain constant with increasing A, until it eventually snaps to zero at the onset of phase trapping (figure 12c: $A = 0.92$). By tracking the ring structure in the Poincaré map (figure 12d), we find a gradual shrinkage of the $\mathbb{T}^2$ attractor en route to lock-in, providing evidence of an inverse Neimark–Sacker bifurcation (Balanov *et al.* 2009). Put together, these
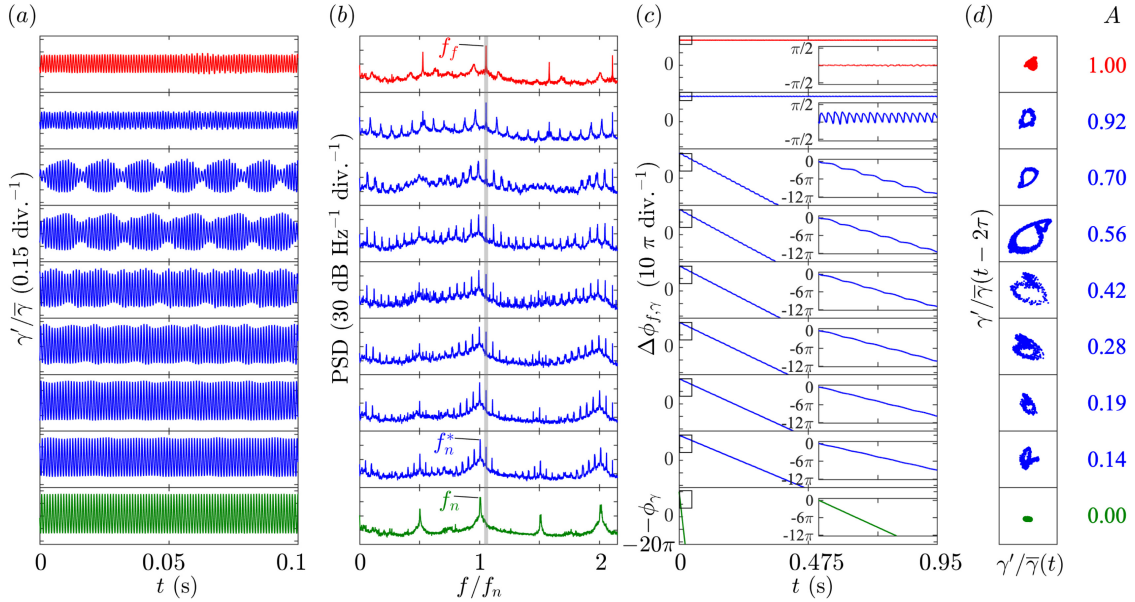
Figure 12: Synchronization dynamics of the jet when forced transversely (position $\mathbb{E}$) at a frequency close to its natural global frequency: $f_f/f_n = 1.04$. The (a) time trace, (b) PSD, (c) temporal evolution of $\Delta\phi_{f,\gamma}$, and (d) one-sided Poincaré map are shown for nine forcing amplitudes, including the unforced case ($A = 0$). Lock-in occurs via the suppression route, which involves a Neimark–Sacker bifurcation at $A = 0 \to 0.14$ followed by an inverse Neimark–Sacker bifurcation at $A = 0.92 \to 1$. The unforced state is shown in green, the quasiperiodic states are shown in blue, and the onset of lock-in is shown in red.
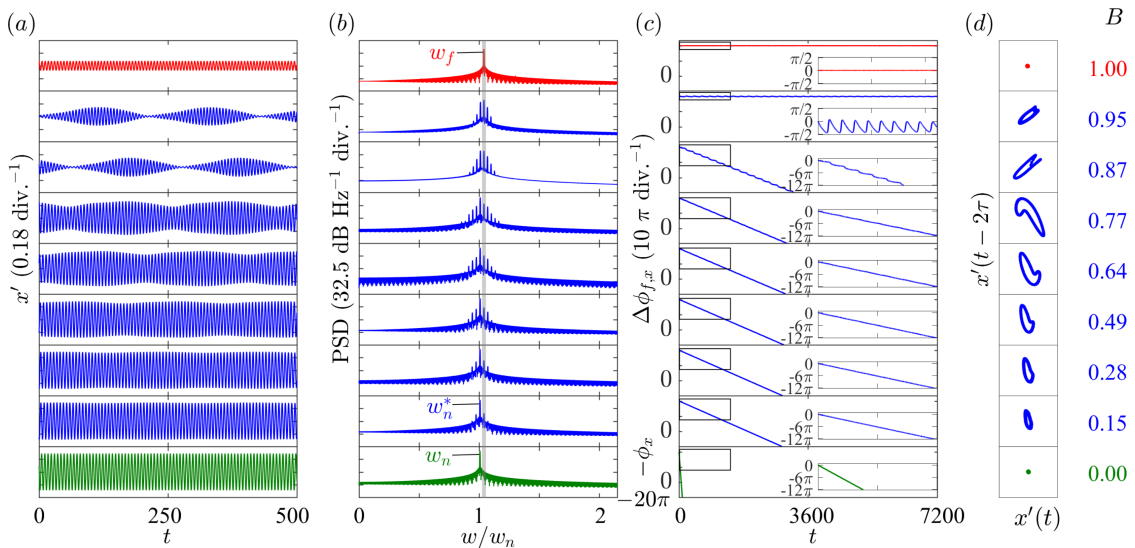

Figure 13: The same as in figure 12 but for the transversely forced model at $\omega_f/\omega_n = 1.04$.

observations reveal that when its axisymmetry is broken via transverse forcing, the jet locks in via the suppression route, even when the detuning is small. This is strikingly different from the phase-locking route taken by the axially forced jet (figure 8). An intrinsic feature of the suppression route is a marked reduction in the oscillation amplitude en route to lock-in (Balanov *et al.* 2009). Here, such a reduction is indeed observed, both in the time trace (figure 12a) and in the synchronization map (figure 5). Figure 13 shows that the main synchronization phenomena exhibited by the transversely forced jet – such as the amplitude
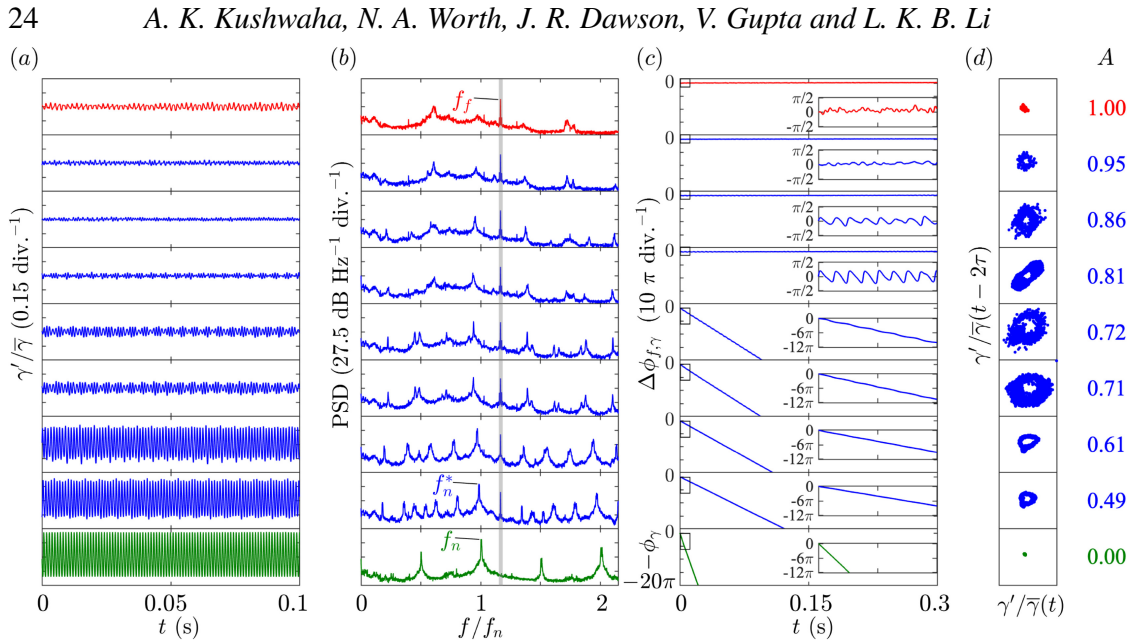
24   *A. K. Kushwaha, N. A. Worth, J. R. Dawson, V. Gupta and L. K. B. Li*

Figure 14: Synchronization dynamics of the jet when forced transversely (position $\mathbb{E}$) at a frequency far from its natural global frequency: $f_f/f_n = 1.17$. The (a) time trace, (b) PSD, (c) temporal evolution of $\Delta\phi_{f,\gamma}$, and (d) one-sided Poincaré map are shown for nine forcing amplitudes, including the unforced case ($A = 0$). Lock-in occurs via the suppression route, which involves a Neimark–Sacker bifurcation at $A = 0 \to 0.49$ followed by an inverse Neimark–Sacker bifurcation at $A = 0.95 \to 1$. The unforced state is shown in green, the quasiperiodic states are shown in blue, and the onset of lock-in is shown in red.
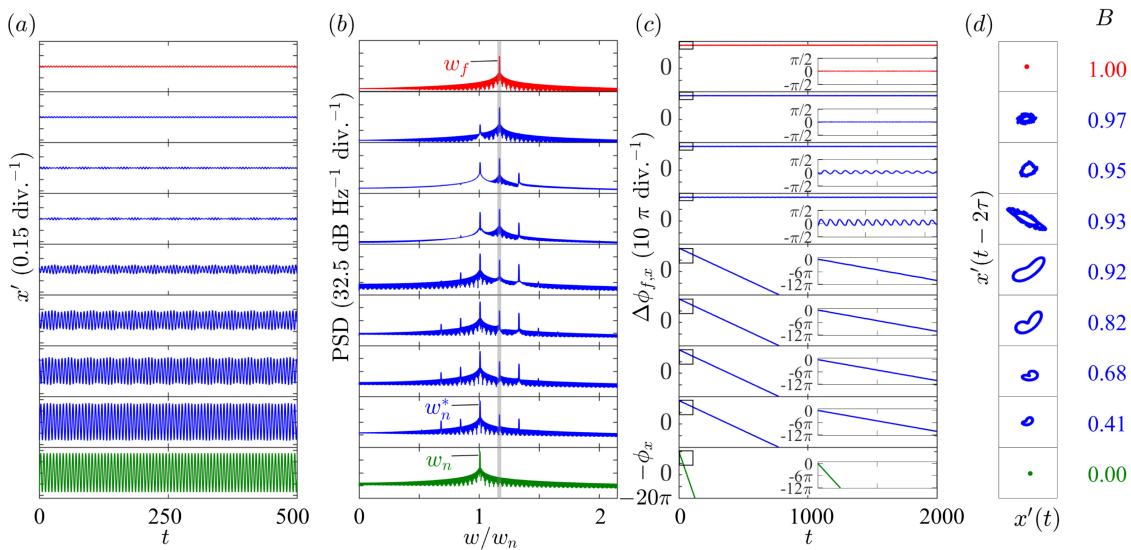

Figure 15: The same as in figure 14 but for the transversely forced model at $\omega_f/\omega_n = 1.17$.

reduction, phase trapping, and suppression route to lock-in via an inverse Neimark–Sacker bifurcation – are well captured by the transversely forced model.

Next we increase f_f so that it is far from f_n (figure 14: $f_f/f_n = 1.17$). We find that the jet responds qualitatively similarly to when f_f is close to f_n (figure 12: $f_f/f_n = 1.04$). Specifically, lock-in still occurs via the suppression route: (i) the natural mode becomes quenched without its frequency f_n^* being pulled towards f_f, (ii) phase trapping occurs just before the onset of lock-in, and (iii) the $\mathbb{T}^2$ attractor shrinks gradually to its death via an inverse Neimark–Sacker bifurcation. For comparison, we show the corresponding model

response in figure 15. As is the case for small detuning (figures 12 and 13), we find that the model can qualitatively reproduce the main synchronization phenomena exhibited by the jet, including the substantial reduction in the oscillation amplitude en route to lock-in (figure 15a).

5.4. *Asynchronous quenching*

In §5.3.1, we showed that when forced axially, the jet locks in via the phase-locking route when the detuning is small, but via the suppression route when the detuning is large. In §5.3.2, we showed that when forced transversely, the jet locks in exclusively via the suppression route, regardless of whether the detuning is small or large. According to synchronization theory based on a self-excited oscillator with a single natural mode (Balanov *et al.* 2009), only the suppression route can cause asynchronous quenching of the natural mode without resonant amplification of the forced mode. The findings of §5.3.1 and §5.3.2 thus suggest that transverse forcing would be more effective than axial forcing in suppressing the global axisymmetric oscillations of a low-density jet. Below we provide definitive evidence of this and show that, like most other synchronization phenomena observed in the jet, asynchronous quenching can be qualitatively reproduced by the coupled oscillator model of §3.

Figure 16 shows the spectral power of the natural mode ($P_n'^*$), of the forced mode ($P_f'^*$), and of the total γ' signal ($P_t'^*$), all as a function of the forcing power (A^2) for both axial and transverse forcing. We consider two representative non-resonant values of f_f, one below f_n (figure 16a,c: $f_f/f_n = 0.82$) and one above f_n (figure 16b,d: $f_f/f_n = 1.17$). Both f_f values are sufficiently far from f_n for lock-in to occur via the suppression route (figure 5). We compute the spectral power by integrating the PSD around each respective mode (± 5 Hz) and then normalizing the result by the total power of the unforced system (P_t'). We compute the total power by integrating the PSD across the entire bandwidth, with verification that it obeys Parseval's theorem, i.e. that it is equal (within 0.22%) to the mean squared fluctuation.

5.4.1. *Axial forcing: the jet at position* $\mathbb{A}$

Figure 16(a,b) shows that, regardless of whether $f_f/f_n < 1$ or > 1, the axially forced jet undergoes a suppression of its natural mode en route to lock-in (grey shading). This is demonstrated by $P_n'^*$ decaying to zero as A^2 increases to 1 and beyond, providing clear evidence of asynchronous quenching (Bogoliubov & Mitropolsky 1961; Minorsky 1967, 1974). Meanwhile, $P_f'^*$ increases but in two different ways. When $f_f/f_n > 1$ (figure 16b), $P_f'^*$ increases linearly with A^2 up to and beyond lock-in. When $f_f/f_n < 1$ (figure 16a), however, $P_f'^*$ increases linearly at first but then nonlinearly at higher A^2 values, jumping sharply at the onset of lock-in ($A^2 = 1$). This accelerated growth in $P_f'^*$ is indicative of an amplification of the forced mode via nonlinear interactions with the natural mode (Odajima *et al.* 1974; Abel *et al.* 2009). Because here the forcing is non-resonant (figure 16a: $f_f/f_n = 0.82$), this phenomenon is referred to as *non-resonant amplification* (Nayfeh & Mook 1995). Such an amplification of the forced mode causes $P_t'^*$ to rise above that of the unforced system ($P_t'^*/P_t' > 1$). Consequently, if the control objective is to suppress the global axisymmetric oscillations of a low-density jet using axial forcing, then it is not simply enough for f_f to be sufficiently far from f_n to activate the suppression route: one must also ensure that $f_f/f_n > 1$, as this enables asynchronous quenching to occur without resonant or non-resonant amplification en route to lock-in (figure 16b). If f_f is somehow allowed to fall below f_n, then asynchronous quenching still occurs, but its effect is counteracted by non-resonant amplification of the forced mode, resulting in the total power increasing above that of the unforced system as lock-in is approached (figure 16a). We believe that this is the first time that asynchronous quenching has been observed alongside non-resonant amplification in a
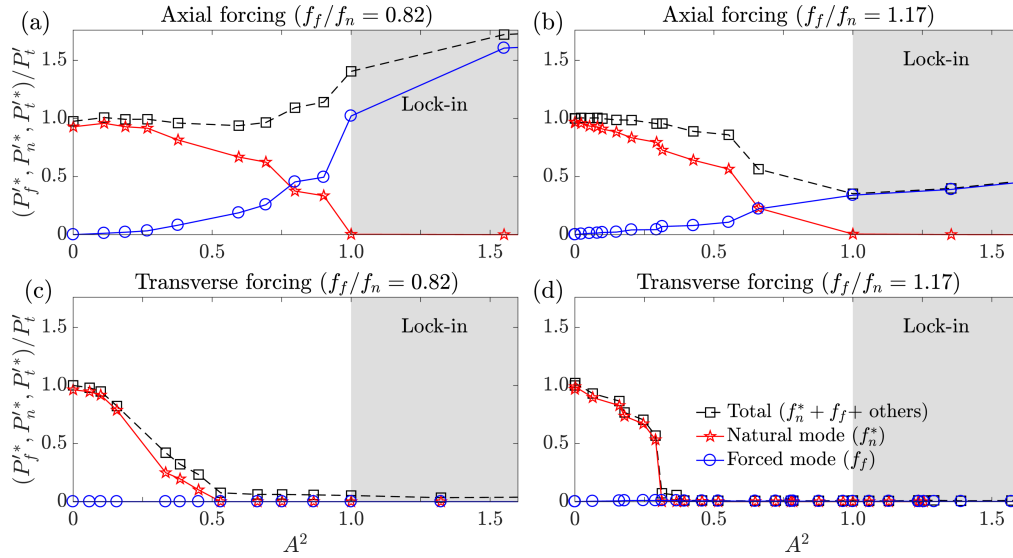
Figure 16: Evidence of asynchronous quenching in the jet: spectral power as a function of the forcing power for (a,b) axial forcing and (c,d) transverse forcing. For both types of forcing, lock-in occurs via the suppression route. Two representative values of f_f are shown, (a,c) one below f_n and (b,d) one above f_n.
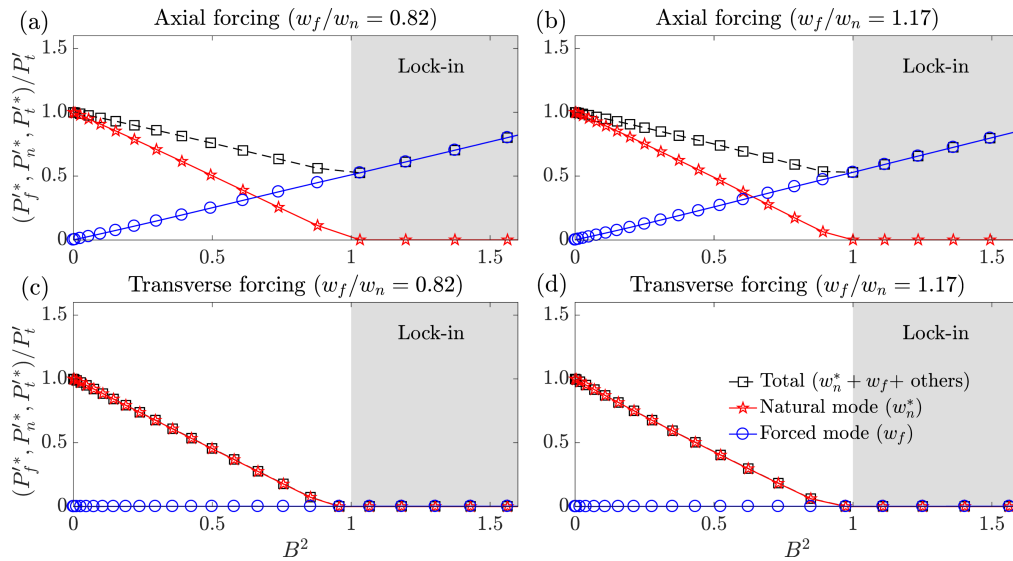

Figure 17: The same as in figure 16 but for the axially or transversely forced model.

forced self-excited hydrodynamic system. As §5.4.2 will confirm, this discovery provides a compelling incentive to consider axisymmetry breaking, via transverse forcing, as an alternative method of suppressing a nonlinear global mode.

Figure 17(a,b) shows the spectral power of the axially forced model at the two forcing frequencies shown in figure 16(a,b): $\omega_f/\omega_n = 0.82$ and 1.17. For both values of ω_f/ω_n, the model can qualitatively capture the asynchronous quenching observed in the jet: P'^*_n decays to zero as B^2 increases to 1 and beyond. However, the model cannot capture the non-resonant amplification of the forced mode, regardless of whether $\omega_f/\omega_n < 1$ or > 1. Instead, it exhibits a proportional relationship between P'^*_f and B^2, resulting in P'^*_t remaining well below that of the unforced state en route to and at the onset of lock-in ($B^2 = 1$). The inability of the model to capture non-resonant amplification when the forcing frequency is

below the natural frequency is why the asymmetry about $f_f/f_n = 1$ in the η_γ data from the jet (figure 5) is absent in the η_x data from the model (figure 6). Nevertheless, in both the jet and the model, continuing to increase the forcing amplitude (or forcing power) after lock-in eventually causes the total amplitude to rise above that of the unforced state (figure 5).

5.4.2. *Transverse forcing: the jet at position* $\mathbb{E}$

Turning now to the transversely forced jet (figure 16c,d), we find that in some ways it behaves similarly to the axially forced jet (figure 16a,b). For example, for both $f_f/f_n < 1$ (figure 16c) and $f_f/f_n > 1$ (figure 16d), $P_n'^*$ decays to zero as A^2 increases. As before, this is clear evidence of asynchronous quenching, consistent with the suppression route to lock-in. However, we find that $P_n'^*$ decays more rapidly here, indicating that transverse forcing is more effective than axial forcing in disrupting the natural global mode of the jet. Moreover, we find that $P_n'^*$ decays to negligible values well before A^2 reaches 1, implying that the onset of natural-mode suppression ($P_n'^* \approx 0$) precedes the onset of lock-in ($A^2 = 1$). This occurs because the onset of lock-in is defined as when the attractor topology changes from $\mathbb{T}^2$ to a periodic orbit. A strong subharmonic mode at $f_n^*/2$ (e.g. see figure 14b) can thus cause the jet to remain quasiperiodic, even when the fundamental mode at f_n^* itself is relatively weak.

Another difference relative to the axially forced jet is that not only is $P_f'^*$ not amplified but it does not even increase in proportion to A^2 (figure 16c,d). Instead, it remains negligible over the entire range of A^2. The complete absence of a response at f_f is in stark contrast to the proportional increase (figure 16b) and the non-resonant amplification (figure 16a) seen in the axially forced jet. These differences suggest that the jet is more receptive to axial perturbations that reinforce the axisymmetry of its natural global mode ($m = 0$) and is less receptive to transverse perturbations that break its axisymmetry ($m = \pm 1$), as expected from the helical hydrodynamic modes ($m = \pm 1$) being only globally stable. Given that $P_f'^* \approx 0$ over the entire range of A^2, $P_t'^*$ decays similarly to $P_n'^*$ for both $f_f/f_n < 1$ and > 1 (figure 16c,d), implying that the overall jet oscillations are quenched well before the onset of lock-in.

Figure 17(c,d) shows that the transversely forced model can qualitatively capture the spectral power characteristics of the transversely forced jet (figure 16c,d). This includes (i) asynchronous quenching of the natural mode, (ii) the absence of any response at the forced mode, and (iii) quenching of the overall jet oscillations to a quiescent state.

5.5. *Synchronous quenching*

To examine the amplitude response at small detuning, we show in figure 18 the spectral power of the jet and of the model for a range of forcing frequencies, both close to and far from the natural frequency. The forcing is either axial or transverse, but always at a relatively low amplitude (see the caption of figure 18).

In the axially forced jet (figure 18a), we find that as f_f/f_n approaches 1 from either the low or high side, $P_n'^*$ decays to zero whilst $P_f'^*$ grows to a maximum. This indicates that synchronous quenching of the natural mode is occurring alongside resonant amplification of the forced mode (Keen & Fletcher 1969; Odajima *et al.* 1974; Abel *et al.* 2009; Mondal *et al.* 2019). Here the degree of resonant amplification is strong enough to enable $P_f'^*$ to counterbalance the quenching of $P_n'^*$, resulting in $P_t'^*$ exceeding P_t' just below $f_f/f_n = 1$. In the axially forced model (figure 18b), we find the same qualitative behaviour involving the simultaneous occurrence of synchronous quenching and resonant amplification when f_f/f_n is close to 1. Similar behaviour has recently been observed in self-excited thermoacoustic systems subjected to similar resonant forcing (Guan *et al.* 2019a,b; Mondal *et al.* 2019). However, we believe that this is the first time that synchronous quenching has been observed

28   *A. K. Kushwaha, N. A. Worth, J. R. Dawson, V. Gupta and L. K. B. Li*
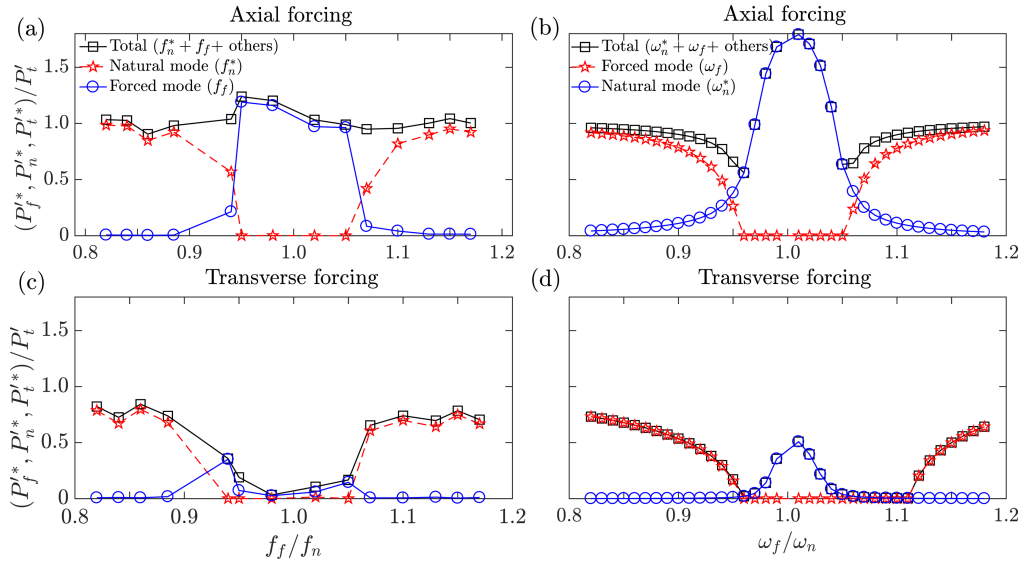

Figure 18: Evidence of synchronous quenching in (a,c) the jet and (b,d) the model: spectral power as a function of the normalized forcing frequency for (a,b) axial forcing and (c,d) transverse forcing. The forcing amplitude is (a) $a = 0.998$ Pa, (b) $b = 0.019$, (c) $a = 1.320$ Pa, and (d) $b = 0.049$.

alongside resonant amplification in a self-excited hydrodynamic system, reinforcing the universality of such synchronization phenomena in physically disparate systems.

In the transversely forced jet (figure 18c), we find markedly different behaviour: although synchronous quenching of the natural mode still occurs ($P_n'^* \to 0$), the forced mode is not amplified to a degree sufficient to cause $P_t'^*$ to exceed P_t', implying the absence of resonant amplification. The same qualitative behaviour is observed in the transversely forced model (figure 18d). This demonstrates that synchronous quenching of the natural mode occurring without resonant amplification of the forced mode is the primary mechanism by which transverse forcing is able to reduce the overall response amplitude when f_f is close to f_n.

6. Conclusions

In this study, we have adopted a forced synchronization framework to answer three research questions (§1.4) on the open-loop control of period-1 limit-cycle oscillations in a prototypical hydrodynamic oscillator, namely a globally unstable low-density axisymmetric jet.

(i) *Can breaking the axisymmetry of the jet via transverse forcing lead to a more effective open-loop control strategy than preserving the axisymmetry via axial forcing?*

We have experimentally shown that breaking the $m = 0$ axisymmetry of the nonlinear global mode of the jet, by applying transverse acoustic forcing (flapping perturbations), can cause lock-in to occur exclusively via the suppression route, regardless of whether f_f is close to or far from f_n. This insensitivity to detuning enables both asynchronous and synchronous quenching of the natural mode to occur without resonant or non-resonant amplification of the forced mode. The result is a substantially greater reduction in the overall response amplitude across all tested values of f_f/f_n, as compared with the baseline case of axial forcing. This shows that simply switching from symmetric to asymmetric perturbations can lead to a more effective open-loop control strategy, in the sense that stronger amplitude suppression can be achieved without the need to worry about the exact detuning between f_f and f_n.

(ii) *How do the synchronization phenomena – such as the bifurcation routes, Arnold tongues, and quenching mechanisms – differ between transverse and axial forcing?*

We have experimentally shown that when applied at low A, transverse forcing, like axial forcing, causes the jet to transition from a period-1 orbit on a limit-cycle attractor to $\mathbb{T}^2$ quasiperiodicity on a torus attractor via a Neimark–Sacker bifurcation. When A increases, however, we find that the subsequent transition, from $\mathbb{T}^2$ quasiperiodicity to 1:1 lock-in, depends on the spatial symmetry of the applied perturbations. Specifically, we find that axial forcing induces a saddle-node bifurcation at small detuning but an inverse Neimark–Sacker bifurcation at large detuning, whereas transverse forcing always induces an inverse Neimark–Sacker bifurcation irrespective of the detuning. Nevertheless, we find that the shape and position of the Arnold tongue remain similar for both types of forcing. This shows that although transverse and axial forcing are equally capable of causing lock-in, only transverse forcing can ensure that it occurs via the suppression route rather than the phase-locking route. It is partly through this specific route selection that transverse forcing can suppress the natural mode via synchronous quenching at small detuning and asynchronous quenching at large detuning, without ever incurring a significant amplification of the forcing signal.

(iii) *Can these synchronization phenomena be modelled phenomenologically with a low-dimensional system based simply on a pair of coupled VDP oscillators?*

We have shown that the main synchronization phenomena exhibited by the jet can be qualitatively modelled with just two generic VDP oscillators coupled to each other and forced externally by sinusoidal terms. The success of such a simple low-dimensional model in capturing the complex nonlinear dynamics of a multi-modal hydrodynamic system opens up the possibility that, with further development, such a model could be used to explore the forced synchronization of other hydrodynamically self-excited flows subjected to axisymmetric and non-axisymmetric mode excitation. As well as offering new insight into the interactions between different hydrodynamic and acoustic modes, this could facilitate the discovery of novel control strategies for the suppression of nonlinear global modes.

Regarding future work, one aspect that deserves further attention is the asymmetry in η_γ about $f_f/f_n = 1$, which was detected in the axially forced jet (figure 5). We believe that this asymmetry may be due to the different spatial-mode structures generated at different values of f_f, with higher frequency modes experiencing stronger viscous damping and thus stronger amplitude attenuation. One of our next steps is to explore this further by extending the present temporal analysis to a spatiotemporal analysis involving a more detailed modal decomposition of the PIV images and low-order modelling via the Ginzburg–Landau equation.

Appendix A. Nonlinear time series analysis

Forced synchronization is an inherently nonlinear process (Pikovsky *et al.* 2003; Balanov *et al.* 2009). As such, it is often studied in phase space (i.e. state space) using methods from nonlinear time series analysis (Kantz & Schreiber 2003). In general, the phase space of a continuous dynamical system is a Q-dimensional hyperspace in which all Q state variables reside. Within this hyperspace, the temporal evolution of the system is represented by its phase trajectory, whose characteristics can reveal useful information about the topology of the

30 *A. K. Kushwaha, N. A. Worth, J. R. Dawson, V. Gupta and L. K. B. Li*

dominant attractors. In most real-world systems, however, it is difficult to determine the phase space directly because not all of its state variables are known or accessible. Nevertheless, owing to intrinsic coupling between different state variables, it is possible to reconstruct the phase space from only a single scalar observation function, by using the time-delay embedding theorem of Takens (1981). Here we use this theorem to reconstruct the dominant attractors as an Euclidean vector of time-delayed elements of dimension q:

$$\xi(t) = [\gamma'(t), \gamma'(t-\tau), \gamma'(t-2\tau), \ldots, \gamma'(t-(q-1)\tau)], \quad \xi \in \mathbb{R}^q, \qquad (A\,1)$$

where γ' is the velocity fluctuation in the jet (this is replaced by x' in the model of §3), τ is the embedding time delay, and q is the embedding dimension. We set the value of τ to be the time taken by the average mutual information function to attain its first local minimum (Fraser & Swinney 1986). This ensures that the time-delayed vector elements are optimally decorrelated such that the attractors unfold maximally in the embedding space, enabling their fine structures to be readily identified (Kantz & Schreiber 2003). We determine the minimum value of q using the algorithm of Cao (1997). After reconstructing the phase space, we visualize the attractors within it in two ways: (i) via the three-dimensional phase portrait and (ii) via a two-dimensional slice through the phase portrait, which is known as the Poincaré map (Kantz & Schreiber 2003).

REFERENCES

ABEL, M., AHNERT, K. & BERGWEILER, S. 2009 Synchronization of sound sources. *Phys. Rev. Lett.* **103** (11), 114301.

ÆSØY, E., AGUILAR, J., WORTH, N. A. & DAWSON, J. R. 2021 The response of an axisymmetric jet placed at various positions in a standing wave. *J. Fluid Mech.* **917**, A16.

ARONSON, D. G., ERMENTROUT, G. B. & KOPELL, N. 1990 Amplitude response of coupled oscillators. *Physica D* **41** (3), 403–449.

BAEK, S. J. & SUNG, H. J. 2000 Quasi-periodicity in the wake of a rotationally oscillating cylinder. *J. Fluid Mech.* **408**, 275–300.

BALANOV, A., JANSON, N., POSTNOV, D. & SOSNOVTSEVA, O. 2009 *Synchronization: From Simple to Complex.* Heidelberg, Germany: Springer–Verlag.

BAUERHEIM, M., SALAS, P., NICOUD, F. & POINSOT, T. 2014 Symmetry breaking of azimuthal thermo-acoustic modes in annular cavities: a theoretical study. *J. Fluid Mech.* **760**, 431–465.

BELLOWS, B. D., HREIZ, A. & LIEUWEN, T. 2008 Nonlinear interactions between forced and self-excited acoustic oscillations in premixed combustor. *J. Propul. Power* **24** (3), 628–631.

BLIMBAUM, J., ZANCHETTA, M., AKIN, T., ACHARYA, V., O'CONNOR, J., NOBLE, D. R. & LIEUWEN, T. 2012 Transverse to longitudinal acoustic coupling processes in annular combustion chambers. *Int. J. Spray. Combust.* **4** (4), 275–297.

BOGOLIUBOV, N. N. & MITROPOLSKY, Y. A. 1961 *Asymptotic Methods in the Theory of Non-Linear Oscillations,* 2nd edn. CRC Press.

BOTHIEN, M. R., NOIRAY, N. & SCHUERMANS, B. 2015 Analysis of azimuthal thermo-acoustic modes in annular gas turbine combustion chambers. *J. Eng. Gas Turb. Power* **137** (6).

BOURGOUIN, J. F., DUROX, D., MOECK, J. P., SCHULLER, T. & CANDEL, S. 2015 Characterization and modeling of a spinning thermoacoustic instability in an annular combustor equipped with multiple matrix injectors. *J. Eng. Gas Turb. Power* **137** (2).

BROZE, G. & HUSSAIN, F. 1994 Nonlinear dynamics of forced transitional jets: Periodic and chaotic attractors. *J. Fluid Mech.* **263**, 93–132.

CAO, L. 1997 Practical method for determining the minimum embedding dimension of a scalar time series. *Physica D* **110** (1), 43–50.

CARTWRIGHT, J. H. E., EGUÍLUZ, V. M., HERNÁNDEZ-GARCÍA, E. & PIRO, O. 1999 Dynamics of elastic excitable media. *Int. J. Bifurcat. Chaos* **9** (11), 2197–2202.

CHAKRAVARTHY, R. V. K., LESSHAFFT, L. & HUERRE, P. 2018 Global stability of buoyant jets and plumes. *J. Fluid Mech.* **835**, 654–673.

CHOMAZ, J. M. 2005 Global instabilities in spatially developing flows: Non-normality and nonlinearity. *Annu. Rev. Fluid Mech.* **37**, 357–392.

CHOMAZ, J. M., HUERRE, P. & REDEKOPP, L. G. 1988 Bifurcations to local and global modes in spatially developing flows. *Phys. Rev. Lett.* **60** (1), 25–28.

COENEN, W., LESSHAFFT, L., GARNAUD, X. & SEVILLA, A. 2017 Global instability of low-density jets. *J. Fluid Mech.* **820**, 187–207.

COENEN, W. & SEVILLA, A. 2012 The structure of the absolutely unstable regions in the near field of low-density jets. *J. Fluid Mech.* **713**, 123–149.

COENEN, W., SEVILLA, A. & SÁNCHEZ, A. L. 2008 Absolute instability of light jets emerging from circular injector tubes. *Phys. Fluids* **20** (7), 074104.

DA SILVA, C. B. & MÉTAIS, O. 2002 Vortex control of bifurcating jets: a numerical study. *Phys. Fluids* **14** (11), 3798–3819.

DANAILA, I. & BOERSMA, B. J. 2000 Direct numerical simulation of bifurcating jets. *Phys. Fluids* **12** (5), 1255–1257.

DAVITIAN, J., GETSINGER, D., HENDRICKSON, C. & KARAGOZIAN, A. R. 2010*a* Transition to global instability in transverse-jet shear layers. *J. Fluid Mech.* **661**, 294–315.

DAVITIAN, J., HENDRICKSON, C., GETSINGER, D., M'CLOSKEY, R. T. & KARAGOZIAN, A. R. 2010*b* Strategic control of transverse jet shear layer instabilities. *AIAA J.* **48** (9), 2145–2156.

DEWAN, E. M. 1972 Harmonic entrainment of van der Pol oscillations: Phaselocking and asynchronous quenching. *IEEE T. Automat. Contr.* **17** (5), 655–663.

DOUGLAS, C. M., EMERSON, B. L., HEMCHANDRA, S. & LIEUWEN, T. C. 2021 Forced flow response analysis of a turbulent swirling annular jet flame. *Phys. Fluids* **33** (8), 085124.

DRAZIN, P. G. & REID, W. H. 2004 *Hydrodynamic Stability*, 2nd edn. Cambridge, England: Cambridge University Press.

FRASER, A. M. & SWINNEY, H. L. 1986 Independent coordinates for strange attractors from mutual information. *Phys. Rev. A* **33** (2), 1134–1140.

GHIRARDO, G. & JUNIPER, M. P. 2013 Azimuthal instabilities in annular combustors: standing and spinning modes. *P. R. Soc. A.* **469** (2157), 20130232.

GHIRARDO, G., JUNIPER, M. P. & MOECK, J. P. 2016 Weakly nonlinear analysis of thermoacoustic instabilities in annular combustors. *J. Fluid Mech.* **805**, 52–87.

GOHIL, T. B. & SAHA, A. K. 2019 Numerical simulation of forced circular jets: Effect of flapping perturbation. *Phys. Fluids* **31** (8), 083602.

GUAN, Y., GUPTA, V., KASHINATH, K. & LI, L. K. B. 2019*a* Open-loop control of periodic thermoacoustic oscillations: experiments and low-order modelling in a synchronization framework. *P. Combust. Inst.* **37** (4), 5315–5323.

GUAN, Y., GUPTA, V., WAN, M. & LI, L. K. B. 2019*b* Forced synchronization of quasiperiodic oscillations in a thermoacoustic system. *J. Fluid Mech.* **879**, 390–421.

GUAN, Y., HE, W., MURUGESAN, M., LI, Q., LIU, P. & LI, L. K. B. 2019*c* Control of self-excited thermoacoustic oscillations using transient forcing, hysteresis and mode switching. *Combust. Flame* **202**, 262–275.

GUAN, Y., MOON, K., KIM, K. T. & LI, L. K. B. 2021 Low-order modeling of the mutual synchronization between two turbulent thermoacoustic oscillators. *Phys. Rev. E* **104** (2), 024216.

GUAN, Y., MURUGESAN, M. & LI, L. K. B. 2018 Strange nonchaotic and chaotic attractors in a self-excited thermoacoustic oscillator subjected to external periodic forcing. *Chaos* **28** (9), 093109.

HALLBERG, M .P., SRINIVASAN, V., GORSE, P. & STRYKOWSKI, P. J. 2007 Suppression of global modes in low-density axisymmetric jets using coflow. *Phys. Fluids* **19** (1), 014102.

HALLBERG, M. P. & STRYKOWSKI, P. J. 2006 On the universality of global modes in low-density axisymmetric jets. *J. Fluid Mech.* **569**, 493–507.

HALLBERG, M. P. & STRYKOWSKI, P. J. 2008 Open-loop control of fully nonlinear self-excited oscillations. *Phys. Fluids* **20** (4), 041703.

HAUSER, M., LORENZ, M. & SATTELMAYER, T. 2010 Influence of transversal acoustic excitation of the burner approach flow on the flame structure. In *ASME Turbo Expo 2010: Power for Land, Sea, and Air*, pp. 803–812.

HUERRE, P. & MONKEWITZ, P. A. 1990 Local and global instabilities in spatially developing flows. *Annu. Rev. Fluid Mech.* **22**, 473–537.

HYODO, H. & BIWA, T. 2018 Phase-locking and suppression states observed in forced synchronization of thermoacoustic oscillator. *J. Phys. Soc. Jpn.* **87** (3), 034402.

32   *A. K. Kushwaha, N. A. Worth, J. R. Dawson, V. Gupta and L. K. B. Li*

JANG, S. H & IH., J. G. 1998 On the multiple microphone method for measuring in-duct acoustic properties in the presence of mean flow. *J. Acoust. Soc. Am.* **103** (3), 1520–1526.

JENDOUBI, S. & STRYKOWSKI, P. J. 1994 Absolute and convective instability of axisymmetric jets with external flow. *Phys. Fluids* **6** (9), 3000–3009.

JUNIPER, M. P. 2012 Absolute and convective instability in gas turbine fuel injectors. In *Proceedings of ASME Turbo Expo*. Copenhagen, Denmark: ASME International Gas Turbine Institute, GT2012-68253.

JUNIPER, M. P., LI, L. K. B. & NICHOLS, J. W. 2009 Forcing of self-excited round jet diffusion flames. *P. Combust. Inst.* **32** (1), 1191–1198.

KANTZ, H. & SCHREIBER, T. 2003 *Nonlinear Time Series Analysis*, 2nd edn. Cambridge, England: Cambridge University Press.

KARAGOZIAN, A. R. 2010 Transverse jets and their control. *Prog. Energ. Combust.* **36** (5), 531–553.

KARNIADAKIS, G. E. & TRIANTAFYLLOU, G. S. 1989 Frequency selection and asymptotic states in laminar wakes. *J. Fluid Mech.* **199**, 441–469.

KASHINATH, K., LI, L. K. B. & JUNIPER, M. P. 2018 Forced synchronization of periodic and aperiodic thermoacoustic oscillations: lock-in, bifurcations and open-loop control. *J. Fluid Mech.* **838**, 690–714.

KEEN, B. E. & FLETCHER, W. H. W 1969 Suppression and enhancement of an ion-sound instability by nonlinear resonance effects in a plasma. *Phys. Rev. Lett.* **23** (14), 760.

KEEN, B. E. & FLETCHER, W. H. W. 1970 Suppression of a plasma instability by the method of 'asynchronous quenching'. *Phys. Rev. Lett.* **24** (4), 130.

KOOPMANN, G. H. 1967 The vortex wakes of vibrating cylinders at low Reynolds numbers. *J. Fluid Mech.* **28** (3), 501–512.

KYLE, D. M. & SREENIVASAN, K. R. 1993 The instability and breakdown of a round variable-density jet. *J. Fluid Mech.* **249**, 619–664.

LEE, M., ZHU, Y.and LI, L. K. B. & GUPTA, V. 2019 System identification of a low-density jet via its noise-induced dynamics. *J. Fluid Mech.* **862**, 200–215.

LESPINASSE, F., BAILLOT, F. & BOUSHAKI, T. 2013 Responses of V-flames placed in an HF transverse acoustic field from a velocity to pressure antinode. *C. R. Mecanique* **341** (1-2), 110–120.

LESSHAFFT, L. & HUERRE, P. 2007 Linear impulse response in hot round jets. *Phys. Fluids* **19** (2), 024102.

LESSHAFFT, L., HUERRE, P. & SAGAUT, P. 2007 Frequency selection in globally unstable round jets. *Phys. Fluids* **19** (5), 054108.

LESSHAFFT, L., HUERRE, P., SAGAUT, P. & TERRACOL, M. 2006 Nonlinear global modes in hot jets. *J. Fluid Mech.* **554**, 393–409.

LESSHAFFT, L. & MARQUET, O. 2010 Optimal velocity and density profiles for the onset of absolute instability in jets. *J. Fluid Mech.* **662**, 398–408.

LI, L. K. B. & JUNIPER, M. P. 2013*a* Lock-in and quasiperiodicity in a forced hydrodynamically self-excited jet. *J. Fluid Mech.* **726**, 624–655.

LI, L. K. B. & JUNIPER, M. P. 2013*b* Lock-in and quasiperiodicity in hydrodynamically self-excited flames: Experiments and modelling. *P. Combust. Inst.* **34** (1), 947–954.

LI, L. K. B. & JUNIPER, M. P. 2013*c* Phase trapping and slipping in a forced hydrodynamically self-excited jet. *J. Fluid Mech.* **735** (R5), 1–11.

LUBARSKY, E., SHCHERBIK, D., BIBIK, A. & ZINN, B. T. 2003 Active control of combustion oscillations by non-coherent fuel flow modulation. In *9th AIAA/CEAS Aeroacoustics Conference and Exhibit*, p. 3180.

LUCERO, J. C. & SCHOENTGEN, J. 2013 Modeling vocal fold asymmetries with coupled van der Pol oscillators. In *Proceedings of Meetings on Acoustics*, , vol. 19, p. 060165. Acoustical Society of America.

MARQUES, F. & LOPEZ, J. M. 2006 Onset of three-dimensional unsteady states in small-aspect-ratio Taylor–Couette flow. *J. Fluid Mech.* **561**, 255–277.

MINORSKY, N. 1967 Comments on 'asynchronous quenching'. *IEEE T. Automat. Contr.* **12** (2), 225–227.

MINORSKY, N. 1974 *Nonlinear Oscillations*. Krieger Publishing.

MONDAL, S., PAWAR, S. A. & SUJITH, R. I. 2019 Forced synchronization and asynchronous quenching of periodic oscillations in a thermoacoustic system. *J. Fluid Mech.* **864**, 73–96.

MONKEWITZ, P. A., BECHERT, D. W., BARSIKOW, B. & LEHMANN, B. 1990 Self-excited oscillations and mixing in a heated round jet. *J. Fluid Mech.* **213**, 611–639.

MONKEWITZ, P. A. & SOHN, K. D. 1988 Absolute instability in hot jets. *AIAA J.* **26** (8), 911–916.

MURUGESAN, M., ZHU, Y. & LI, L. K. B. 2019 Complex network analysis of forced synchronization in a hydrodynamically self-excited jet. *Int. J. Heat Fluid Flow* **76**, 14–25.

NAYFEH, A. H. & MOOK, D. T. 1995 *Nonlinear Oscillations*. New York, NY, USA: John Wiley & Sons.

NOIRAY, N., BOTHIEN, M. & SCHUERMANS, B. 2011 Investigation of azimuthal staging concepts in annular gas turbines. *Combust. Theor. and Model.* **15** (5), 585–606.

NOIRAY, N. & SCHUERMANS, B. 2013*a* Deterministic quantities characterizing noise driven hopf bifurcations in gas turbine combustors. *Int. J. Nonlin. Mech.* **50**, 152–163.

NOIRAY, N. & SCHUERMANS, B. 2013*b* On the dynamic nature of azimuthal thermoacoustic modes in annular gas turbine combustion chambers. *Proc. R. Soc. A* **469** (2151), 20120535.

OBERLEITHNER, K., STÖHR, M., IM, S. H., ARNDT, C. M. & STEINBERG, A. M. 2015 Formation and flame-induced suppression of the precessing vortex core in a swirl combustor: experiments and linear stability analysis. *Combust. Flame* **162** (8), 3100–3114.

O'CONNOR, J., ACHARYA, V. & LIEUWEN, T. 2015 Transverse combustion instabilities: acoustic, fluid mechanic, and flame processes. *Prog. Energ. Combust.* **49**, 1–39.

O'CONNOR, J. & LIEUWEN, T. 2011 Disturbance field characteristics of a transversely excited burner. *Combust. Sci. Technol.* **183** (5), 427–443.

O'CONNOR, J. & LIEUWEN, T. 2012 Further characterization of the disturbance field in a transversely excited swirl-stabilized flame. *J. Eng. Gas. Turb. Power* **134** (1), 011501.

O'CONNOR, J. & LIEUWEN, T. 2012 Recirculation zone dynamics of a transversely excited swirl flow and flame. *Phys. fluids* **24** (7), 2893–2900.

ODAJIMA, K., NISHIDA, Y. & HATTA, Y. 1974 Synchronous quenching of drift-wave instability. *Phys. Fluids* **17** (8), 1631–1633.

OHE, K. & TAKEDA, S. 1974 Asynchronous quenching and resonance excitation of ionization waves in positive columns. *Beit. Plasmaphys.-Cont.* **14** (2), 55–65.

OLINGER, D. J. 1992 Lock-in states in the dripping mode of the capillary jet. *Exp. Fluids* **15** (2), 155–158.

OLINGER, D. J. & SREENIVASAN, K. R. 1988 Nonlinear dynamics of the wake of an oscillating cylinder. *Phys. Rev. Lett.* **60** (9), 797–800.

PAREKH, D., REYNOLDS, W. & MUNGAL, M. 1987 Bifurcation of round air jets by dual-mode acoustic excitation. In *25th AIAA Aerospace Sciences Meeting*, p. 164.

PIKOVSKY, A. S., ROSENBLUM, M. G. & KURTHS, J. 2003 *Synchronization: A Universal Concept in Nonlinear Sciences*. Cambridge, England: Cambridge University Press.

VAN DER POL, B. 1926 On relaxation oscillations. *Phil. Mag.* **2** (11), 978–992.

PROVANSAL, M., MATHIS, C. & BOYER, L. 1987 Bénard-von Kármán instability: Transient and forced regimes. *J. Fluid Mech.* **182**, 1–22.

QADRI, U. A., CHANDLER, G. J. & JUNIPER, M. P. 2018 Passive control of global instability in low-density jets. *Eur. J. Mech. B. Fluids* **72**, 311–319.

REYNOLDS, W. C., PAREKH, D. E., JUVET, P. J. D. & LEE, M. J. D. 2003 Bifurcating and blooming jets. *Annu. Rev. Fluid Mech.* **35** (1), 295–315.

REYNOLDS, W. C. & POTTER, M. C. 1967 Finite-amplitude instability of parallel shear flows. *J. Fluid Mech.* **27** (3), 465–492.

RIGAS, G., JAMIESON, N. P., LI, L. K. B. & JUNIPER, M. P. 2016 Experimental sensitivity analysis and control of thermoacoustic systems. *J. Fluid Mech.* **787**, R1.

ROWLEY, C. W. & DAWSON, S. T. M. 2017 Model reduction for flow analysis and control. *Annu. Rev. Fluid Mech.* **49**, 387–417.

ROY, A., MONDAL, S., PAWAR, S. A. & SUJITH, R. I. 2020 On the mechanism of open-loop control of thermoacoustic instability in a laminar premixed combustor. *J. Fluid Mech.* **884**, A2.

SAURABH, A., MOECK, J. P. & PASCHEREIT, C. O. 2017 Swirl flame response to simultaneous axial and transverse velocity fluctuations. *J. Eng. Gas Turb. Power* **139** (6), 061502.

SAURABH, A. & PASCHEREIT, C. O. 2017 Dynamics of premixed swirl flames under the influence of transverse acoustic fluctuations. *Combust. Flame* **182**, 298–312.

SCHMID, P. J. 2010 Dynamic mode decomposition of numerical and experimental data. *J. Fluid Mech.* **656**, 5–28.

SCHMID, P. J. & HENNINGSON, D. S. 2001 *Stability and Transition in Shear Flows*. Springer.

SCHMID, P. J., HENNINGSON, D. S. & JANKOWSKI, D. F. 2002 Stability and transition in shear flows. *Appl. Mech. Rev.* **55** (3), B57–B59.

34   *A. K. Kushwaha, N. A. Worth, J. R. Dawson, V. Gupta and L. K. B. Li*

SEYBERT, A. F. & ROSS, D. F. 1977 Experimental determination of acoustic properties using a two-microphone random-excitation technique. *J. Acoust. Soc. Am.* **61** (5), 1362–1370.

SHOJI, T., HARRIS, E. W., BESNARD, A., SCHEIN, S. G. & KARAGOZIAN, A. R. 2020 Transverse jet lock-in and quasiperiodicity. *Phys. Rev. Fluids* **5** (1), 013901.

SIPP, D. & LEBEDEV, A. 2007 Global stability of base and mean flows: a general approach and its applications to cylinder and open cavity flows. *J. Fluid Mech.* **593**, 333–358.

SMITH, T., EMERSON, B., PROSCIA, W. & LIEUWEN, T. 2018*a* Role of induced axial acoustics in transverse acoustic flame response. *Combust. Flame* .

SMITH, T. E., DOUGLAS, C. M., EMERSON, B. L. & LIEUWEN, T. C. 2018*b* Axial evolution of forced helical flame and flow disturbances. *J. Fluid Mech.* **844**, 323–356.

SREENIVASAN, K. R., RAGHU, S. & KYLE, D. 1989 Absolute instability in variable density round jets. *Exp. Fluids* **7** (5), 309–317.

SRINIVASAN, V., HALLBERG, M. P. & STRYKOWSKI, P. J. 2010 Viscous linear stability of axisymmetric low-density jets: Parameters influencing absolute instability. *Phys. Fluids* **22** (2), 024103.

STANSBY, P. K. 1976 The locking-on of vortex shedding due to the cross-stream vibration of circular cylinders in uniform and shear flows. *J. Fluid Mech.* **74** (4), 641–665.

STAUBLI, T. & ROCKWELL, D. 1987 Interaction of an unstable planar jet with an oscillating leading edge. *J. Fluid Mech.* **176**, 135–167.

STROGATZ, S. H. 1994 *Nonlinear Dynamics and Chaos*. New York, NY, USA: Perseus Books.

SUZUKI, H., KASAGI, N. & SUZUKI, Y. 2004 Active control of an axisymmetric jet with distributed electromagnetic flap actuators. *Exp. Fluids* **36** (3), 498–509.

TAKENS, F. 1981 Detecting strange attractors in turbulence. In *Dynamical Systems and Turbulence, Lecture Notes in Mathematics* (ed. D. A. Rand & L. S. Young), , vol. 898, pp. 366–381. New York, NY, USA: Springer–Verlag.

TAMMISOLA, O. & JUNIPER, M. P. 2016 Coherent structures in a swirl injector at $Re = 4800$ by nonlinear simulations and linear global modes. *J. Fluid Mech.* **792**, 620–657.

THÉVENIN, J., ROMANELLI, M., VALLET, M., BRUNEL, M. & ERNEUX, T. 2011 Resonance assisted synchronization of coupled oscillators: Frequency locking without phase locking. *Phys. Rev. Lett.* **107** (10), 104101.

TYLISZCZAK, A. 2015 Multi-armed jets: A subset of the blooming jets. *Phys. Fluids* **27** (4), 041703.

TYLISZCZAK, A. & GEURTS, B. J. 2014 Parametric analysis of excited round jets – Numerical study. *Flow Turbul. Combust.* **93** (2), 221–247.

URBIN, G. & MÉTAIS, O. 1997 Large-eddy simulations of three-dimensional spatially-developing round jets. In *Direct and Large-Eddy Simulation II*, pp. 35–46. Springer.

WELCH, P. D. 1967 The use of Fast Fourier Transform for the estimation of power spectra: A method based on time averaging over short modified periodograms. *IEEE. T. Acoust. Speech* **15**, 70–73.

WOLF, P., STAFFELBACH, G., GICQUEL, L. Y. M., MÜLLER, J. & POINSOT, T. 2012 Acoustic and large eddy simulation studies of azimuthal modes in annular combustion chambers. *Combust. Flame* **159** (11), 3398–3413.

WORTH, N. A. & DAWSON, J. R. 2013 Self-excited circumferential instabilities in a model annular gas turbine combustor: Global flame dynamics. *P. Combust. Inst.* **34** (2), 3127–3134.

WORTH, N. A., MISTRY, D., BERK, T. & DAWSON, J. R. 2020 Vortex dynamics of a jet at the pressure node in a standing wave. *J. Fluid Mech.* **882**, A22.

YANG, D., LAERA, D. & MORGANS, A. S. 2019 A systematic study of nonlinear coupling of thermoacoustic modes in annular combustors. *J. Sound Vib.* **456**, 137–161.

YU, M. H. & MONKEWITZ, P. A. 1990 The effect of nonuniform density on the absolute instability of two-dimensional inertial jets and wakes. *Phys. Fluids A* **2** (7), 1175–1181.

ZHU, Y., GUPTA, V. & LI, L. K. B. 2017 Onset of global instability in low-density jets. *J. Fluid Mech.* **828**, R1.

ZHU, Y., GUPTA, V. & LI, L. K. B. 2019 Coherence resonance in low-density jets. *J. Fluid Mech.* **881**, R1.